Microbiology, Metabolites and Biotechnology
Journal home page:
MMB
The former ARMMT

Green-synthesized nickel oxide nanoparticles from tea: A dual-action antibiofilm and anti-quorum-sensing activity against selected foodborne pathogens

Maryam Basbus Khanevaneh, Mirsasan Mirpour , Mohammad Faezi Ghasemi*, Behnam Rasti

Department of Microbiology, La.C., Islamic Azad University, Lahijan, Iran.

Article Info

Document Type:
Research Paper

Received 13/08/2026
Received in revised form 01/10/2026
Accepted 04/10/2026

Published 11/06/2026

Keywords:
Nickel oxide nanoparticles,
Green synthesis,
Quorum sensing-associated gene expression,
Biofilm inhibition,
Foodborne pathogens

Abstract

Foodborne pathogens pose a persistent threat to public health due to their ability to form biofilms and regulate virulence through quorum sensing (QS). This study evaluated the antibacterial, antibiofilm, and QS-inhibitory activities of nickel oxide nanoparticles (NiONPs) green-synthesized using black tea (NiONPs-BT) and green tea (NiONPs-GT) extracts against *Staphylococcus aureus*, *Escherichia coli*, and *Listeria monocytogenes*. Nanoparticles were comprehensively characterized using UV-Visible spectroscopy, X-ray diffraction (XRD), Dynamic light scattering (DLS), zeta potential analysis, Fourier transform infrared (FTIR), transmission electron microscopy (TEM), and scanning electron microscopy (SEM). Antibacterial activity was assessed via minimum inhibitory concentration (MIC) and minimum bactericidal concentration (MBC) assays, while biofilm inhibition was evaluated using the crystal violet method at sub-MIC and MIC concentrations. Changes in gene expression of biofilm- and QS-related genes were analyzed by quantitative real-time PCR (qPCR). NiONPs-BT exhibited superior colloidal stability (-44.4 mV) and a larger crystallite size (31.3 nm) compared to NiONPs-GT (-20.7 mV; 29.8 nm). Notably, biofilm inhibition reached up to 92.3% with NiONPs-BT against *L. monocytogenes* at MIC, with substantial inhibition observed even at sub-MIC concentrations. qPCR analysis revealed significant downregulation of key virulence genes, including *icaA* (0.084-fold), *csgD* (0.21-fold), and *agrB* (0.06-fold), indicating transcriptional interference with biofilm and QS-associated regulatory networks. These findings demonstrate that tea-mediated NiONPs, particularly NiONPs-BT, effectively inhibit biofilm formation and suppress the expression of QS-associated and biofilm-related genes, suggesting their potential as anti-virulence agents by indirect mechanisms. This sustainable, phytochemical-based nano strategy needs further investigation as a potential alternative for addressing biofilm persistence and QS-regulated virulence. However, comprehensive toxicity studies should be considered before any food industry-related applications.

1. Introduction

Foodborne pathogens continue to pose a significant threat to public health and food safety, causing substantial morbidity, mortality, and economic losses worldwide (Elmegdar *et al.*, 2024; Lawal *et al.*, 2025). Among these pathogens, *Staphylococcus aureus*, *Escherichia coli* and *Listeria monocytogenes* are of particular concern due to their ability to survive in food-processing environments and persist on surfaces (Alavi *et al.*, 2025). A key factor contributing to their persistence is biofilm formation produced by an extracellular matrix. Biofilms provide enhanced resistance to antimicrobial agents and environmental stressors, complicating eradication efforts in food production settings (Dsouza *et al.*, 2024).

Biofilm development is tightly regulated by quorum sensing (QS), a bacterial cell-to-cell communication system that coordinates gene expression in response to population density (Bilici *et al.*, 2025; Boban *et al.*, 2023). QS systems, such as the agr operon in Gram-positive pathogens (*S. aureus* and *L. monocytogenes*) and the *luxS*/AI-2 system in *E. coli*, control key processes including adhesion, virulence factor production, and biofilm maturation (Hindieh *et al.*, 2025). Targeting QS has emerged as a promising strategy to disrupt biofilms while minimizing selective pressure for resistance development (Şensoy Gün *et al.*, 2025). However, it is important to distinguish between direct quorum-quenching activity (e.g., signal molecule degradation or receptor antagonism) and indirect suppression of QS-associated gene expression, as these represent mechanistically distinct phenomena.

The widespread use of conventional antimicrobials and chemical disinfectants in food-related environments has

MMB In Press

*Corresponding author E-mail: mfaezi@iau.ac.ir, faezi_m@yahoo.com
DOI: 10.22104/mmb.2026.8491.1212 https://mmb.irost.ir/article_1761.html

COPYRIGHTS: © 2026. Authors retain the copyright and full publishing rights.

Published by Iranian Research Organization for Science and Technology (IROST). This article is an open access article licensed under the Creative Commons Attribution 4.0 International (CC BY 4.0) (https://creativecommons.org/licenses/by/4.0/)

raised concerns about antimicrobial resistance, chemical residues, and potential human health risks (Jangid *et al.*, 2025). Nanotechnology offers promising alternatives, with metal oxide nanoparticles, particularly NiONPs, demonstrating broad-spectrum antimicrobial activity, chemical stability, and suitability for surface applications (Khan *et al.*, 2022). However, the biological performance and safety of these nanoparticles strongly depend on their synthesis methods and surface chemistry.

Green synthesis using plant extracts offers an eco-friendly and sustainable approach, where phytochemicals act as both reducing and stabilizing agents, thereby influencing nanoparticle size, morphology, and surface properties (Afrasiabi *et al.*, 2025; Qais *et al.*, 2021). Tea (*Camellia sinensis*) is particularly rich in bioactive polyphenols that serve dual roles in nanoparticle synthesis: (i) as reducing agents for Ni^{2+} to Ni^{0}, and (ii) as capping/stabilizing agents that control nucleation and growth kinetics. However, the polyphenolic profile differs fundamentally between tea types due to post-harvest processing. Green tea retains high concentrations of native catechins (epigallocatechin gallate, EGCG; epicatechin gallate, ECG; epigallocatechin, EGC; and epicatechin, EC), which possess multiple ortho-dihydroxyl groups that enable strong metal chelation and radical scavenging (Cao *et al.*, 2025; Spaggiari, 2025). In contrast, black tea undergoes enzymatic oxidation (fermentation), converting catechins into higher-molecular-weight theaflavins and thearubigins through oxidative polymerization (Tanaka *et al.*, 2016). These structural differences have profound implications for nanoparticle synthesis: Catechins (green tea) exhibit higher reducing potential due to their B-ring catechol groups ($E° \sim 0.3\text{-}0.5$ V), enabling rapid nucleation and formation of smaller crystallites (Parvathalu *et al.*, 2023; Rasheed & Jum'a, 2026). Theaflavins (black tea), while still redox-active, have lower reducing capacity due to electron delocalization across the benzotropolone ring system, potentially slowing nucleation kinetics (Tanaka *et al.*, 2016). Although the extracts themselves were not chemically characterized in the present study, such relationships are considered hypothetical (Parvathalu *et al.*, 2023; Rasheed & Jum'a, 2026; Tanaka *et al.*, 2009).

Although green-synthesized NiONPs have demonstrated antimicrobial activity, most studies have focused on single-plant extracts without systematically comparing how phytochemical diversity influences nanoparticle properties and bioactivity. For instance, Kalita *et al.* (2021) synthesized NiO NPs using *Camellia sinensis* extract, reporting an average particle size of 2 nm and efficient antimicrobial activity against both Gram-positive and Gram-negative bacteria. To date, only a few reports have explored tea-mediated NiONPs (Khalifa, 2025; Tian *et al.*, 2026), and none have directly compared black versus green tea extracts to dissect the structure-activity relationships governing antibacterial and anti-quorum sensing efficacy. Comparative studies examining NiONPs derived from different tea types and their effects on quorum sensing (QS)-regulated biofilm formation remain scarce. Furthermore, while several reports have described the antimicrobial activity of green-synthesized metal oxide nanoparticles, few have systematically compared how distinct tea phytochemical profiles influence QS inhibition and the transcriptional regulation of biofilm-associated genes.

To address this gap, this study investigated the antibiofilm activity of NiONPs green-synthesized using black and green tea extracts against selected foodborne pathogens including *S. aureus*, *E. coli*, and *L.* monocytogenes, and examined their effects on the expression of QS-associated and biofilm-related genes. Antimicrobial activity, biofilm inhibition at sub-inhibitory and minimum inhibitory concentrations (MIC), and transcriptional changes in key QS and biofilm-related genes were assessed. The comparative approach employed in this study provides a foundation for optimizing green synthesis strategies to develop next-generation antimicrobial nanomaterials tailored for food safety applications. It is important to emphasize that this study is intended as a preliminary in vitro screening investigation. The primary objective is to compare the physicochemical properties and biological activities of NiONPs derived from two distinct tea sources, rather than to propose immediate food-contact or food-preservation applications. Comprehensive biosafety assessments, including mammalian cytotoxicity and metal migration/leaching studies, are beyond the scope of the present work but are essential prerequisites for any application.

2. Materials and Methods

2.1. Plant extract preparation

Green and black tea leaves (*Camellia sinensis*; herbarium voucher No. IMPH609) were obtained from the Medicinal Plant Research Center, Jahad Daneshgahi, Karaj, Iran. The dried leaves were separately ground to a fine powder using a mechanical grinder and kept in airtight glass containers at room temperature, protected from light, until extraction. Ethanolic extracts were prepared by maceration. Briefly, 10 g of powdered green or black tea leaves were mixed separately with 100 mL of 96% ethanol at a solid-to-solvent ratio of 1:10 (w/v). The mixtures were kept at room temperature in the dark for 7 days and stirred occasionally throughout the extraction period. The extracts were then passed through Whatman No. 1 filter paper to remove plant residues. The filtrates were collected in amber glass bottles and stored at 4°C until use in nanoparticle synthesis.

To ensure batch-to-batch consistency of the plant extracts used for nanoparticle synthesis, each extract batch was subjected to comprehensive phytochemical characterization prior to use. Total phenolic content (TPC) was determined using the Folin-Ciocalteu method, expressed as gallic acid equivalents (GAE) per gram of dry extract (Singleton & Rossi, 1965). Total flavonoid content (TFC) was measured using the aluminum chloride colorimetric method, expressed as quercetin equivalents (QE) per gram of dry extract (Zhishen *et al.*, 1999). The antioxidant capacity was assessed using the DPPH (2,2-diphenyl-1-picrylhydrazyl) radical scavenging assay, with IC_{50} values calculated as the extract concentration required to scavenge 50% of DPPH radicals (Brand-Williams *et al.*, 1995). Only extract batches with TPC, TFC, and DPPH IC_{50} values within ±5% of the mean were used for nanoparticle synthesis to ensure batch-to-batch

consistency (Brand-Williams *et al.*, 1995; Rasheed & Jum'a, 2026; Zhishen *et al.*, 1999).

For determination of extraction yield, an aliquot of each filtrate was concentrated by solvent evaporation under reduced pressure at 40°C, and the yield was calculated gravimetrically as the percentage of dry extract relative to the initial mass of plant material (Sharma *et al.*, 2024).

2.2. Green Synthesis of NiONPs

Nickel oxide nanoparticles (NiONPs) were prepared using a precipitation-assisted green synthesis approach, in which tea extracts were used as plant-derived stabilizing and surface-capping agents (Qais *et al.*, 2021). For each synthesis batch, freshly prepared extract was used within 24 hours to minimize oxidative degradation of polyphenolic compounds. Nickel nitrate hexahydrate [Ni $(NO_3)_2$•$6H_2O$; ≥99.0% purity; CAS No. 13478-00-7; Merck, Darmstadt, Germany] was used as the nickel precursor without further purification. A 0.1 M stock solution was prepared by dissolving 29.08 g of Ni $(NO_3)_2$•$6H_2O$ in 1 L of deionized water (resistivity ≥18.2 MΩ/cm; Millipore Direct-Q UV, Merck, Germany). The exact concentration was verified by inductively coupled plasma optical emission spectrometry (ICP-OES; Thermo Scientific iCAP 7400, USA) and adjusted if necessary. The precursor solution was stored in an amber glass bottle at 4°C and used within 48 hours of preparation to prevent hydrolysis. Prior to each synthesis, the pH of the precursor solution was measured and adjusted to 6.0 ± 0.1 using 0.1 M HNO_3 or 0.1 M NaOH if required.

For each synthesis batch, 90 mL of the 0.1 M nickel nitrate precursor solution was transferred to a 250 mL three-neck round-bottom flask equipped with a magnetic stirrer, reflux condenser, and temperature probe. The solution was heated to 60°C ± 0.5°C using a temperature-controlled heating mantle (IKA C-MAG HS 10, Germany) with continuous stirring at 600 ± 10 rpm. Once thermal equilibrium was achieved (typically after 15-20 minutes), 10 mL of standardized tea extract (either green or black tea, prepared as described in Section 2.1) was added dropwise at a rate of 1 mL/min using a peristaltic pump (Masterflex L/S, Cole-Parmer, USA) to ensure controlled addition. The addition rate was selected based on preliminary optimization experiments (data not shown) to prevent localized supersaturation and ensure homogeneous nucleation.

Following complete extract addition, the reaction mixture pH was adjusted to 10.0 ± 0.1 using 1 M NaOH (prepared from analytical grade pellets; Merck, Germany) added dropwise under continuous stirring. pH was monitored throughout using a calibrated pH meter (Mettler Toledo SevenCompact S210, Switzerland) equipped with a temperature-compensated electrode. The pH adjustment was performed slowly over approximately 10-15 minutes, with continuous monitoring until the target pH was stabilized for at least 5 minutes. The formation of a greenish-blue precipitate was observed immediately upon pH adjustment, consistent with the formation of nickel hydroxide [$Ni(OH)_2$] as an intermediate precursor, as confirmed by preliminary XRD analysis (data not shown).

The reaction mixture was maintained at 60°C ± 0.5°C for 2 hours under continuous stirring at 600 ± 10 rpm, during which the precipitate gradually darkened, indicating the progression of nickel hydroxide to nickel oxide formation. The reaction vessel was covered with aluminum foil to minimize photochemical degradation of polyphenolic compounds. Temperature stability was confirmed by continuous monitoring using a digital thermometer with ±0.1°C accuracy, with temperature fluctuations maintained within ±0.5°C throughout the reaction period.

The precipitate was recovered by centrifugation at 10,000 rpm for 20 min and washed three times with distilled water, followed by washing with ethanol to remove residual soluble components and loosely associated phytochemicals. The recovered material was dried at 80°C for 12 h. The dried precursor was then calcined at 400°C for 3 h in a muffle furnace to obtain NiONPs (Sajid *et al.*, 2026). The final nanoparticle yield was determined gravimetrically. The resulting NiONPs powders prepared using green and black tea extracts were stored in airtight vials at 4°C until physicochemical characterization and antibacterial evaluation.

2.3. Characterization of NiONPs

The biosynthesized NiONPs were characterized using multiple complementary techniques to evaluate their physicochemical properties. UV-visible spectroscopy (UV-Vis, Shimadzu UV-1800, Japan) was performed over the wavelength range of 200–800 nm to confirm nanoparticle formation and determine the optical band gap. X-ray diffraction (XRD, Bruker D8 Advance, Germany) with Cu-Kα radiation (λ = 1.5406 Å) was employed to analyze the crystal structure and phase purity of the nanoparticles, operating at 40 kV and 40 mA over a 2θ range of 10°–80° (Bhosale *et al.*, 2025; Hassan *et al.*, 2023).

Dynamic light scattering (DLS) and zeta potential measurements were conducted using a Zetasizer Nano ZS (Malvern Instruments, UK) to determine the hydrodynamic size distribution, polydispersity index (PDI), and surface charge of the nanoparticles dispersed in deionized water at 25°C with a scattering angle of 173°. Zeta potential was measured using the same instrument under identical dispersion conditions. All measurements were performed in triplicate. (Bhattacharjee *et al.*, 2019). Fourier transform infrared (FTIR) spectroscopy (PerkinElmer Spectrum Two, USA) was performed in the range of 400–4000 cm^{-1} using the KBr pellet method to identify the functional groups involved in nanoparticle stabilization and capping (Karthik *et al.*, 2018). Transmission electron microscopy (TEM, Philips CM120, Netherlands) and scanning electron microscopy (SEM, MIRA3 TESCAN, Czech Republic) were employed to examine the morphology, particle size, and surface characteristics of the nanoparticles (Al-Shehri *et al.*, 2024; Karthik *et al.*, 2018). For TEM analysis, nanoparticles were dispersed in ethanol, dropped onto carbon-coated copper grids, and air-dried before imaging. SEM samples were prepared by dispersing the nanoparticles on double-sided carbon tape and sputter-coating them with gold to improve conductivity (Sankar *et al.*, 2023).

2.4. Bacterial strains and culture conditions

Reference strains of *Staphylococcus aureus* PTCC 1784, *Escherichia coli* PTCC 1399, and *Listeria monocytogenes* PTCC 1294 were used for evaluation of the antibacterial activity of the synthesized NiONPs. The lyophilized cultures were obtained from the Persian Type Culture Collection (PTCC), Tehran, Iran, as specified by the culture supplier. Each lyophilized bacterial preparation was reconstituted in 0.5 mL of sterile Tryptic Soy Broth (TSB; Merck, Germany) and incubated at 37°C for 2 h with gentle agitation at 150 rpm.

The resulting suspensions were streaked onto Tryptic Soy Agar (TSA) plates and incubated at 37°C for 18–24 h. Well-isolated colonies were subsequently transferred to fresh TSB and cultured until the mid-logarithmic growth phase, corresponding to an optical density of approximately 0.5 at 600 nm ($OD_{600} \approx 0.5$). For short-term maintenance, bacterial cultures were kept on TSA slants at 4°C, whereas long-term stocks were prepared in TSB containing 20% glycerol and stored at −80°C (Alavi *et al.*, 2025).

2.5. Minimum inhibitory concentration (MIC) and minimum bactericidal concentration (MBC) determination

The MICs of NiONPs synthesized using black tea (NiONPs-BT) and green tea (NiONPs-GT) extracts were determined by the broth microdilution method in 96-well microtiter plates, following CLSI principles (Flentie *et al.*, 2019; Organization, 2022). Overnight bacterial cultures were adjusted to 0.5 McFarland and diluted in Mueller–Hinton Broth (MHB) to obtain a final inoculum of approximately 5×10^5 CFU/mL.

Two-fold serial dilutions of each nanoparticle preparation were tested at final concentrations of 12.5-100 µg/mL in a final volume of 200 µL per well. Untreated bacterial cultures and sterile MHB served as growth and sterility controls, respectively.

Blanks contained the corresponding nanoparticle preparation in MHB without bacteria and were processed identically to the test wells. The OD_{600} of each nanoparticle-only blank was subtracted from the OD_{600} of the corresponding treated well to obtain the corrected bacterial growth. Following incubation at 37°C for 24 h, bacterial growth was assessed visually and by measuring optical density at 600 nm (Balouiri *et al.*, 2016).

The MIC was defined as the lowest nanoparticle concentration showing no detectable bacterial growth relative to the untreated control. For MBC determination, aliquots from wells showing no visible growth at the MIC and higher concentrations were subcultured onto Mueller–Hinton Agar and incubated at 37°C for 24 h. The MBC was defined as the lowest concentration producing no detectable growth following subculture, corresponding to a ≥99.9% reduction in viable bacteria under the assay conditions (Wiegand *et al.*, 2008).

The MBC/MIC ratio was calculated to characterize the antibacterial effect, with ratios ≤4 and >4 interpreted as bactericidal and bacteriostatic, respectively (Pankey & Sabath, 2004). All assays included three independent biological replicates with technical replicate wells, and MIC/MBC values were reported as modal values across independent experiments.

2.6. Growth Curve Analysis at Sub-MIC Concentrations

To evaluate that the concentrations used in biofilm and gene expression assays were truly subinhibitory (i.e., did not significantly affect planktonic growth), growth curves were performed for all bacterial strains in the presence of ¼ MIC and ½ MIC concentrations of NiONPs-BT and NiONPs-GT. Bacterial cultures were inoculated at approximately 5×10^5 CFU/mL in 96-well microtiter plates containing the corresponding nanoparticle concentrations. Growth was monitored by measuring OD_{600} every 2 hours for 24 hours using a microplate reader (BioTek, USA). The specific growth rate (µ) was calculated during the exponential phase using the formula: $\mu = (\ln OD_2 - \ln OD_1)/(t_2 - t_1)$. Only concentrations that resulted in <20% reduction in specific growth rate compared to untreated controls were considered truly subinhibitory and used for downstream biofilm and gene expression assays.

2.7. Biofilm formation assay

The effects of NiONPs-BT and NiONPs-GT nanoparticles on bacterial biofilm formation were evaluated using the crystal violet microtiter plate assay, based on the method described by Stepanović *et al.* (2000), with minor modifications (Stepanović *et al.*, 2000). Three independent biological replicates (n = 3) were performed using freshly prepared bacterial cultures and freshly synthesized nanoparticle batches. The ¼ MIC and ½ MIC concentrations of each nanoparticle preparation were used as sub-inhibitory treatment concentrations. These concentrations were selected to evaluate effects on biofilm formation while minimizing the possibility that marked growth inhibition would be the primary cause of reduced biofilm biomass. The MIC concentration was also included as an additional treatment condition to assess the effect of the inhibitory concentration on the total adherent biomass. Fresh bacterial cultures were adjusted to a 0.5 McFarland standard and diluted in appropriate culture medium. A total volume of 200 µL was added to each well of sterile, flat-bottom 96-well polystyrene microplates, containing the bacterial inoculum and the corresponding concentration of NiONPs-BT or NiONPs-GT. Untreated bacterial cultures served as the biofilm growth control, whereas wells containing sterile culture medium without bacteria served as negative controls. The plates were incubated statically at 37°C for 24 h to allow biofilm formation. Following incubation, planktonic cells were carefully removed without disturbing the attached biomass. The wells were washed three times with 200 µL of sterile phosphate-buffered saline (PBS; pH 7.4) to remove loosely attached and non-adherent cells (O'Toole, 2011). The remaining adherent biomass was fixed with 100 µL of methanol for 15 min at room temperature.

After removal of the methanol, 100 µL of 0.1% (w/v) crystal violet solution was added to each well and incubated for 15 min at room temperature. Excess stain was removed by washing the wells with distilled water,

MMB In Press

after which the plates were allowed to air-dry at room temperature for approximately 30 min. The retained crystal violet was then solubilized by adding 200 µL of 95% ethanol to each well. Absorbance was measured at 570 nm using a microplate reader (BioTek, USA). Biofilm inhibition was calculated relative to the untreated bacterial control using the following equation:

$$\text{Biofilm inhibition (\%)} = \frac{OD_{control} - OD_{treated}}{OD_{control}} \times 100 \quad (1)$$

where $OD_{control}$ represents the absorbance of the untreated bacterial culture, and $OD_{treated}$ represents the absorbance of the corresponding nanoparticle-treated culture. Each experimental condition was analyzed using technical replicate wells in three independent biological experiments. Data were expressed as mean ± standard deviation (SD) (O'Toole, 2011; Stepanović *et al.*, 2000).

To correct any minor differences in bacterial growth that might affect biofilm formation, the biofilm OD values were normalized to the planktonic cell density in the corresponding wells. Planktonic cell density was estimated by transferring 100 µL of the supernatant (after gentle shaking) to a fresh 96-well plate and measuring OD_{600} before staining. This normalization accounts for any slight variations in bacterial growth that may occur even at sub-inhibitory concentrations, ensuring that the reported biofilm inhibition reflects specific effects on biofilm formation rather than indirect effects through growth reduction (O'Toole, 2011; Stepanović *et al.*, 2000).

2.8. RNA Extraction and qPCR

The effects of NiONPs-BT and NiONPs-GT nanoparticles on the expression of selected biofilm-associated and quorum-sensing genes were assessed by quantitative real-time PCR (RT-qPCR).

To minimize transcriptional changes attributable to growth inhibition, exponentially growing bacterial cultures were exposed to ½ MIC of each nanoparticle preparation for 24 h at 37°C with shaking at 150 rpm. Untreated cultures maintained under identical conditions served as controls. Cells were harvested by centrifugation at 8,000 × g for 10 min at 4°C, and total RNA was extracted using the RNeasy Mini Kit (Qiagen, Hilden, Germany) with on-column DNase treatment according to the manufacturer's instructions. RNA concentration and purity were assessed using a NanoDrop 2000 spectrophotometer (Thermo Fisher Scientific, Waltham, MA, USA), and RNA integrity was examined by electrophoresis on 1.2% agarose gels. Samples with A260/A280 ratios of approximately 1.8–2.0 and acceptable RNA integrity were used for cDNA synthesis.

First-strand cDNA was generated from 1 µg of total RNA using the RevertAid First Strand cDNA Synthesis Kit (Thermo Fisher Scientific, Belgium) with random hexamer primers. No-reverse-transcription controls were included to monitor genomic DNA contamination. Primer sequences and expected amplicon sizes are provided in Table 1. Primers were either designed using Primer3 (version 4.1.0) or obtained from published studies. Primer specificity was evaluated by BLAST analysis against the NCBI nucleotide database to confirm that each primer pair targeted only the intended gene sequence. Additionally, melting-curve analysis was performed after each qPCR run to verify the presence of a single amplification product (Figure 9). Primer amplification efficiencies were determined from serial 10-fold dilutions of cDNA (1:1, 1:10, 1:100, 1:1000) using the slope of the standard curve. The efficiency (E) was calculated using the equation E = 10^(−1/slope) − 1. Only primer pairs with efficiencies within the range of 90–110% were used for quantitative analysis. The R^2 values for all standard curves were ≥0.99, indicating strong linearity (Bustin *et al.*, 2009).

Table 1. Primer Sequences of the Selected Bacterial Genes used for qPCR

Strain	Gene	Primer Sequence (5′ → 3′)	Amplicon Size (bp)	Reference
Strain	16S rRNA	F: TTAGCTAGTTGGTAGGGTAATGGC R: CAGTACTTTACGATCCGAAAACCT	145	(Wagner *et al.*, 2020)
S. aureus	*icaA*	F: ACAGTCGCTACGAAAAGAAA R: GGAAATGCCATAATGACAAC	103	(Solati *et al.*, 2015)
	icaD	F: AAGCCAGACAGAGGCAATATCCA R: AGTACAAACAAACTCATCCATCCGA	249	(Greco, 2008)
	agrA	F: TGATAATCCTTATGAGGTGCTT R: CACTGTGACTCGTAACGAAAA	164	(Lopes *et al.*, 2021)
E. coli	*csgD*	F: GCAGGAAGAGTACGGCAAAA R: GACGGTCTGACGAAGAAGGT	175	(Pérez-Lavalle *et al.*, 2023)
	fimH	F: GGTATTACCTCTCCGGCACA R: GTGCGTAATTCGCCGTTAAT	192	(Magdy *et al.*, 2026)
	luxS	F: ACGCCATTACCGTTAAGATG R: AGTGATGCCAGAAAGAGGGA	150	(Kim *et al.*, 2017)
L. monocytogenes	*agrA*	F: CCAACTAATGTAAAATATGAACAT R: ATTCCTTATGTCAGAAATATTTGC	124	(Rieu *et al.*, 2007)
	agrB	F: GTTTGTGCTTGCCCCATTTG R: ATTAGCGTCCCTATCATCGC	183	(Duru *et al.*, 2021)
	agrD	F: GCAAATATTTCTGACATAAGGAAT R: TCAACCACCGCCACCCCCAGAT	121	(Rieu *et al.*, 2007)
	rpoB	F: CGAAGAAGTTGGTCAAGCGTA R: GCCTGTTCAGGTAAACTCCTT	118	(Rieu *et al.*, 2007)

RT-qPCR was performed on a CFX96 Real-Time PCR Detection System (Bio-Rad, Hercules, CA, USA) using SYBR Green chemistry. Each 20-µL reaction contained 10 µL of SYBR Green master mix, 0.5 µM of each primer, 2 µL of diluted cDNA, and nuclease-free water. Cycling conditions were 95°C for 3 min, followed by 40 cycles of 95°C for 15 s, 60°C for 30 s, and 72°C for 30 s. A melting-curve analysis was performed after amplification to confirm product specificity. No-template controls and no-reverse-transcription controls were included in each run. Relative transcript levels were calculated using the comparative $2^{-\Delta\Delta Ct}$ method (Livak & Schmittgen, 2001), with normalization to the corresponding reference gene. The 16S rRNA gene was used as the reference for *S. aureus* and *E. coli*, whereas *rpoB* was used for *L. monocytogenes*. The selection of these reference genes was based on their constitutive expression and prior validation in the respective bacterial species under nanoparticle exposure conditions. Briefly, the Ct values of the target genes were normalized to the Ct values of the reference gene (16S rRNA or rpoB) to obtain ΔCt. The ΔCt of treated samples was then normalized to the ΔCt of untreated control samples to obtain ΔΔCt. Fold change was calculated as $2^{-\Delta\Delta Ct}$. A fold change of <1 indicates downregulation, while a fold change of >1 indicates upregulation relative to the untreated control. Three independent biological replicates were analyzed for each condition, with each sample evaluated in technical triplicate.

2.9. Statistical analysis

Data are presented as mean ± standard deviation (SD) from three independent biological replicates, with technical replicates where applicable. Data distribution and homogeneity of variance were assessed using the Shapiro–Wilk and Levene's tests, respectively. Differences among multiple groups were analyzed using one-way or two-way ANOVA, followed by Tukey's multiple-comparison test. Comparisons between two groups were performed using an unpaired Student's t-test when parametric assumptions were met.

3. Results and Discussion

3.1. UV–Visible Spectroscopic Analysis of NiONPs Synthesized Using Black and Green Tea Extracts

UV–visible spectroscopy was used to examine the optical characteristics of the NiONPs synthesized with black tea (NiONPs-BT) and green tea (NiONPs-GT) extracts as shown in Figure 1A and B. Both samples showed strong absorption in the ultraviolet region, with the main absorption maximum occurring at 325 nm for NiONPs-BT and 309 nm for NiONPs-GT. The corresponding absorbance values were 2.584 and 2.574, respectively. These absorption features are consistent with the characteristic UV absorption reported for NiONPs prepared by plant-mediated approaches. Kalita *et al.* (2021) reported a UV absorption maximum at 346 nm for NiONPs synthesized using *C. sinensis* extract, together with nanoscale particle formation confirmed by electron microscopy (Kalita *et al.*, 2021).

The two samples showed a clear difference in the position of their absorption maxima. The 16-nm shift toward shorter wavelengths observed for NiONPs-GT reflects differences in particle size, surface chemistry, or the nature of phytochemicals associated with the nanoparticle surface. However, UV–visible spectroscopy alone does not allow these factors to be distinguished unequivocally. Therefore, the observed shift is considered an indication of different optical characteristics rather than direct evidence of a specific particle-size difference.

The NiONPs-BT spectrum also showed an additional absorption feature around 260 nm. Because this band was not observed as a distinct maximum in the NiONPs-GT spectrum, it may be related to differences in the organic constituents retained on the nanoparticle surface or to the optical contribution of extract-derived compounds. Such differences are plausible because black and green teas have substantially different polyphenolic profiles. Green tea retains relatively high levels of native catechins, whereas the oxidation process involved in black tea production leads to the formation of compounds such as theaflavins and thearubigins (Cao *et al.*, 2025; Spaggiari, 2025).

The absorption characteristics of metal oxide nanoparticles in the UV region are influenced by several factors, including quantum confinement effects (which become significant below ~10 nm), surface plasmon resonance (less pronounced for NiO compared to noble metals), and the presence of surface-bound phytochemicals that may contribute to the absorption profile (Haase *et al.*, 2018). In the present study, the particle sizes (29.8-31.3 nm) exceed the quantum confinement regime for NiO (typically <10 nm), suggesting that the observed spectral differences are more likely attributable to variations in the phytochemical capping layer composition rather than solely to particle size effects (El-Kemary *et al.*, 2021; Kalita *et al.*, 2021). The additional absorption feature at ~260 nm in the NiONPs-BT spectrum, absent as a distinct maximum in NiONPs-GT, likely originates from theaflavin-derived chromophores retained on the nanoparticle surface, consistent with the different polyphenolic profiles of black and green teas (Tanaka *et al.*, 2016).

3.2. X-ray diffraction (XRD) analysis

X-ray diffraction analysis was performed to confirm the crystal structure and phase purity of the biosynthesized NiONPs (Figure 2). Both NiONPs-BT and NiONPs-GT exhibited characteristic diffraction peaks at 2θ values of 37.2°, 43.3°, and 62.9°, corresponding to the (111), (200), and (220) crystal planes of the face-centered cubic (FCC) structure of nickel oxide. These peaks are in good agreement with the standard JCPDS card No. 47-1049 for

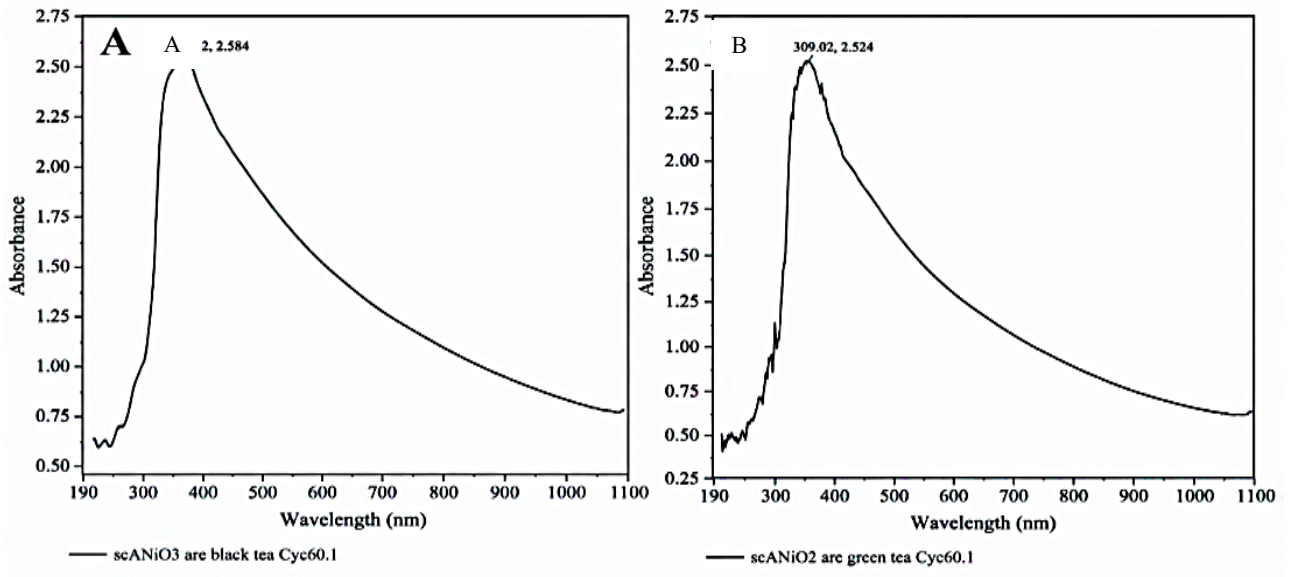


Figure 1. UV-visible absorption spectra of NiONPs synthesized using (A) black tea extract (NiONPs-BT) and (B) green tea extract (NiONPs-GT). Characteristic absorption peaks at 325 nm (NiONPs-BT) and 309 nm (NiONPs-GT) showed the formation of NiONPs. (**Note.** Characteristic absorption peaks at 325 nm (NiONPs-BT) and 309 nm (NiONPs-GT) showed the formation of NiONPs.)

cubic NiONPs (Bhosale *et al.*, 2025; Hassan *et al.*, 2023). The diffraction peaks were sharp and well-resolved, indicating high crystallinity and well-ordered lattice organization of the synthesized nanoparticles. No additional peaks indicative of impurity phases or secondary products were detected, confirming that the green synthesis route using both black and green tea extracts yielded phase-pure NiONPs. Similar findings have been reported for NiONPs synthesized using Olea europaea leaf extract by Al-Shehri *et al.* (2025) and using Azadirachta indica extract by Karthik *et al.* (2022), both of which demonstrated pure cubic phase formation without detectable contaminants (Al-Shehri *et al.*, 2024; Karthik *et al.*, 2018). The average crystallite size was calculated using the Debye-Scherrer equation: $D = K\lambda/(\beta\cos\theta)$, where D is the crystallite size, K is the shape factor (0.9), λ is the X-ray wavelength (1.5406 Å), β is the full width at half-maximum (FWHM) in radians, and θ is the Bragg angle (Scherrer, 1918). The crystallite sizes were estimated from the most intense peak (200) and found to be approximately 31.3 nm for NiONPs-BT and 29.8 nm for NiONPs-GT. The slightly smaller crystallite size observed for NiONPs-GT is consistent with the UV-Vis blue shift (Section 3.1). It suggests that the higher concentration of low-molecular-weight catechins in green tea effectively limits crystal growth during nucleation and synthesis stages, as similarly reported by Rasheed *et al.* (2022) and Parvathalu *et al.* (2023). In contrast, black tea polyphenols, containing higher molecular weight theaflavins and thearubigins, may promote slower nucleation and allow for more extensive crystal growth, resulting in larger crystallite sizes. The crystallite sizes obtained in the present study are consistent with those reported for NiONPs synthesized using *Camellia sinensis* extract (9–15 nm) by Kalita *et al.* (2021) and for plant-mediated NiONPs generally (7–25 nm) as reviewed by Mahmud and Rahman (2025). The high crystallinity and phase purity of the nanoparticles are expected to contribute to their physicochemical stability, which is a critical factor for their biological performance and reproducibility in antimicrobial applications (El-Kemary *et al.*, 2021; Kaur, 2018). Previous studies have demonstrated that plant-mediated synthesis consistently yields highly crystalline metal oxide nanoparticles, with the phytochemicals acting as effective reducing and capping agents that simultaneously direct crystal growth and prevent agglomeration (Sankar *et al.*, 2023; Sati *et al.*, 2025). The absence of impurity peaks further confirms that the biosynthesis process was effective in producing high-purity NiONPs without the need for additional purification steps, which is advantageous for sustainable nanomaterial production (Qais *et al.*, 2021; Uddin *et al.*, 2021).

In the present study, the close correspondence between XRD crystallite sizes (29.8-31.3 nm) and TEM primary particle diameters (29-38 nm) suggests that the NiONPs are predominantly single-crystalline or composed of few crystallites. This interpretation is supported by the sharp, well-resolved XRD peaks, which indicate high crystallinity and minimal lattice strain, as well as the relatively narrow size distribution observed in TEM micrographs. The slightly smaller crystallite size compared to TEM particle size (e.g., 31.3 nm vs. 33-38 nm for NiONPs-BT) is consistent with the presence of a surface layer of amorphous phytochemicals (capping agents) that contributes to the TEM-measured diameter but does not diffract X-rays (Hassan *et al.*, 2023; Sankar *et al.*, 2023).

3.3. Dynamic light scattering (DLS) and zeta potential analysis

Dynamic light scattering (DLS) analysis was performed to evaluate the hydrodynamic particle-size distribution of the biosynthesized NiO nanoparticles using green and black tea extracts, as illustrated in Figure 3(A) and (B). The nanoparticles synthesized using green tea extract (NiONPs-GT) exhibited a primary particle-size peak centered at approximately 390 nm, with a PDI of 0.219. In contrast, the nanoparticles synthesized using black tea-

MMB In Press

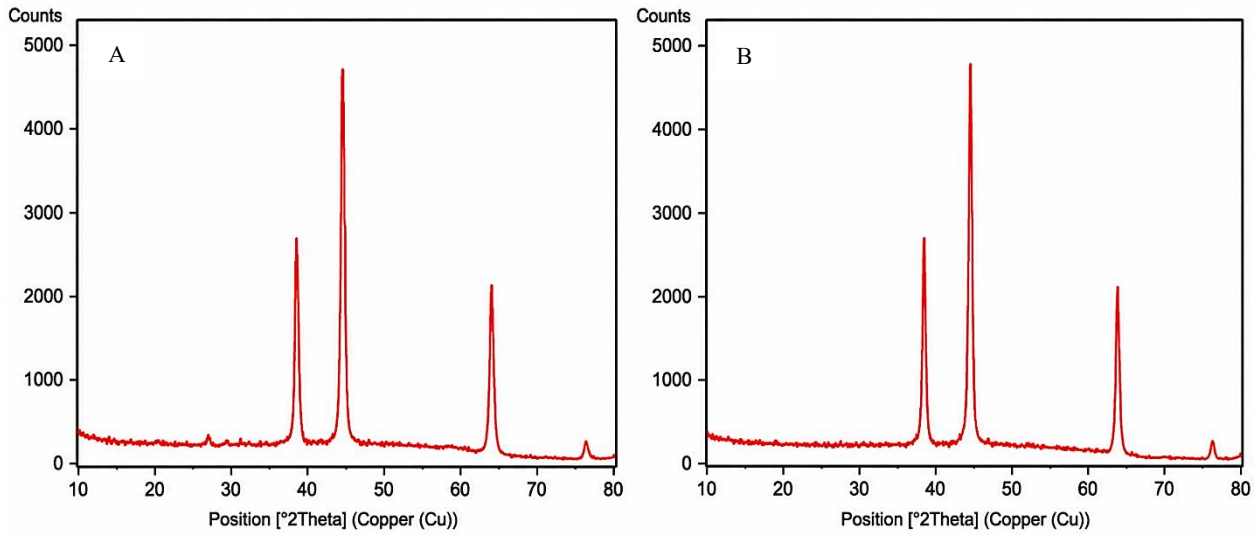


Figure 2. X-ray diffraction patterns of NiONPs synthesized using (A) black tea extract (NiONPs-BT) and (B) green tea extract (NiONPs-GT). (**Note.** Characteristic peaks at 2θ = 37.2°, 43.3°, and 62.9° correspond to the (111), (200), and (220) planes of cubic NiONPs (JCPDS No. 47-1049). The sharp, well-resolved peaks showed high crystallinity and phase purity.)

extract (NiONPs-BT) exhibited a primary particle-size peak at 277.6 nm, with a notably narrower distribution compared to NiONPs-GT and a PDI of 0.325. Therefore, the nanoparticles derived from black tea had a smaller characteristic hydrodynamic size and a significantly narrower size distribution than those derived from green tea. Overall, the DLS results suggest that the type of botanical precursor significantly influences the hydrodynamic size distribution of the biosynthesized NiO nanoparticles. NiONPs-BT demonstrated a smaller characteristic particle size and a more uniform size distribution, whereas NiONPs-GT exhibited a broader distribution extending to larger hydrodynamic diameters. These differences likely arise from variations in the phytochemical composition of the tea extracts and their interactions with the NiO nanoparticle surfaces during the biosynthesis process. (Mukhopadhyay *et al.*, 2025; Sati *et al.*, 2025).

This pattern is consistent with earlier research showing that increased surface charge can boost antimicrobial activity by enhancing interactions with bacterial cells and promoting the production of reactive oxygen species (El-Kemary *et al.*, 2021; Kaur, 2018). Overall, these results highlight the critical role of choosing the right plant source in green nanoparticle synthesis, as it greatly affects the nanoparticles' physical, chemical, and biological characteristics (Qais *et al.*, 2021; Uddin *et al.*, 2021).

This pattern is consistent with earlier research showing that increased surface charge can boost antimicrobial activity by enhancing interactions with bacterial cells and promoting the production of reactive oxygen species (El-Kemary *et al.*, 2021; Kaur, 2018). Overall, these results highlight the critical role of choosing the right plant source in green nanoparticle synthesis, as it greatly affects the nanoparticles' physical, chemical, and biological characteristics (Qais *et al.*, 2021; Uddin *et al.*, 2021).

This degree of polydispersity has several potential implications for the biological performance of the nanoparticles. First, it may influence their penetration into biofilm matrices; second, high PDI can compromise dispersion stability by promoting differential sedimentation and aggregation over time; and third, the coexistence of multiple particle size populations could lead to heterogeneous interactions with bacterial cells and biofilm components, potentially contributing to the multi-targeted transcriptional effects. Zeta potential measurements showed a significantly more negative surface charge for NiONPs-BT (-44.4 mV) compared to NiONPs-GT (-20.7 mV), indicating superior colloidal stability for NiONPs-BT (Bhattacharjee *et al.*, 2016), as shown in Figure 4. The higher absolute zeta potential of NiONPs-BT enhances electrostatic repulsion, preventing particle aggregation and promoting better dispersion in aqueous media (Zheng *et al.*, 2011). The observed difference likely reflects the distinct phytochemical compositions of black and green tea extracts, with black tea polyphenols providing more effective capping and stabilization (Tahir *et al.*, 2024; Rasheed *et al.*, 2022). However, direct evidence linking specific phytochemicals to the measured zeta potentials is not provided in this study. The enhanced colloidal stability of NiONPs-BT correlates with its superior antibacterial activity in liquid culture (Section 3.6), consistent with previous reports demonstrating that nanoparticles with higher surface charges exhibit improved antimicrobial performance through enhanced interaction with bacterial cells and increased reactive oxygen species production (El-Kemary *et al.*, 2021; Kaur, 2018). The hydrodynamic diameters measured by DLS were larger than the primary particle -

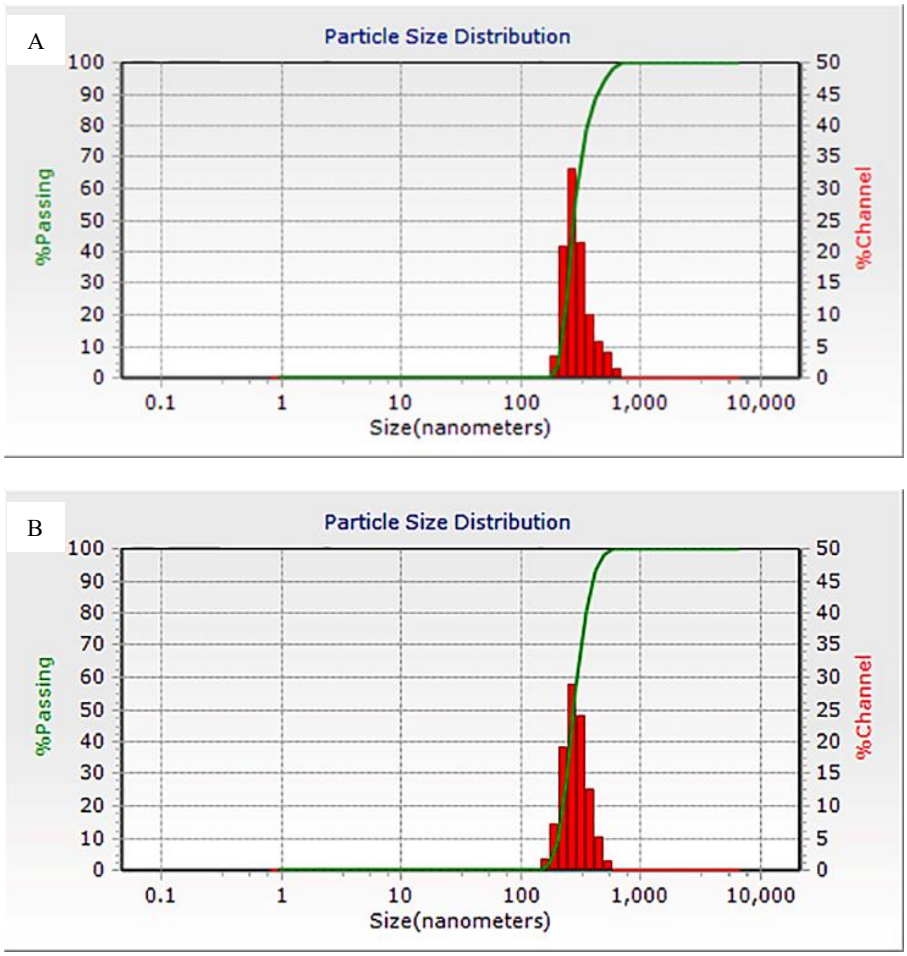


Figure 3. Dynamic light scattering (DLS) particle-size distribution of biosynthesized NiO nanoparticles (A) using green tea and (B) using black tea extracts. (**Note.** Red bars represent the particle-size frequency distribution, whereas the green curves represent the cumulative percentage distribution. NiONPs-GT exhibited a predominant particle-size peak at 390 nm, and NiONPs-BT showed a predominant peak at 277.6 nm. PDI values were 0.219 and 0.325 for NiONPs-GT and NiONPs-BT, respectively.)

sizes observed by TEM (Section 3.5), as DLS measures the hydrated radius including the capping layer and aggregates, while TEM measures the physical core diameter (Hassan *et al.*, 2023; Sankar *et al.*, 2023). These findings highlight the importance of botanical source selection in green nanoparticle synthesis for achieving desired physicochemical and biological properties (Qais *et al.*, 2021; Uddin *et al.*, 2021).

Zeta potential measurements showed a more negative surface charge for NiONPs-BT (−44.4 mV) than for NiONPs-GT (−20.7 mV), suggesting a greater contribution of electrostatic repulsion to the colloidal stabilization of NiONPs-BT (Bhattacharjee *et al.*, 2016). The higher magnitude of the zeta potential may reduce the tendency of nanoparticles to approach and aggregate, thereby favoring their dispersion in aqueous media (Zheng *et al.*, 2011). The observed difference may be related to differences in the phytochemical composition of the black and green tea extracts and their interactions with the nanoparticle surface during biosynthesis. Although black tea-derived phytochemicals may contribute to surface capping and stabilization, the present study does not provide direct evidence linking specific phytochemical constituents to the measured zeta potential values (Tahir *et al.*, 2024; Rasheed *et al.*, 2022).

3.4. Fourier transform infrared (FTIR) spectroscopy Analysis

Fourier transform infrared (FTIR) spectroscopy was employed to identify the functional groups involved in the biosynthesis, stabilization, and capping of NiONPs (Figure 5). The FTIR spectra of both NiONPs-BT and NiONPs-GT exhibited a broad, intense peak at 3200–3400 cm^{-1}, attributed to O–H stretching vibrations of phenolic hydroxyl groups from tea polyphenols (Sankar *et al.*, 2023; Hassan *et al.*, 2021). Peaks observed at 1630–1650 cm^{-1} were assigned to aromatic C=O and C=C stretching vibrations, while absorption bands at 1000–1100 cm^{-1} corresponded to C–O stretching vibrations of alcohols and polyphenolic compounds (Kalita *et al.*, 2021; Rasheed & Jum'a, 2026).

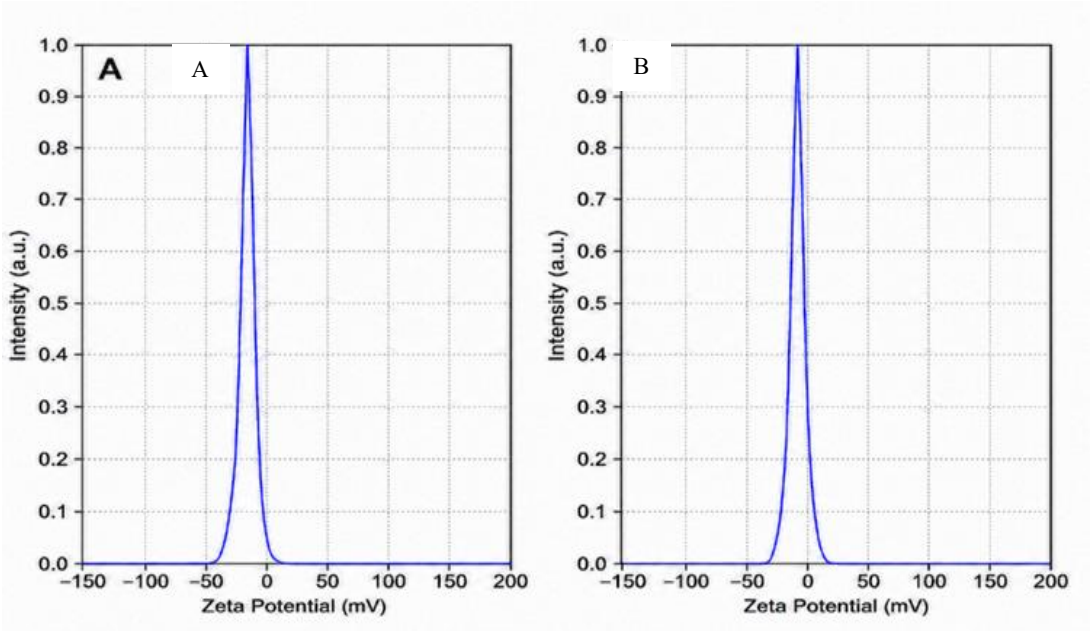


Figure 4. Zeta potential measurements of biosynthesized NiO nanoparticles. (A) NiONPs-BT synthesized using black tea extract and (B) NiONPs-GT synthesized using green tea extract. (**Note.** The measured zeta potentials were −44.4 mV for NiONPs-BT and −20.7 mV for NiONPs-GT. Data are presented as mean ± SD (n = 3).)

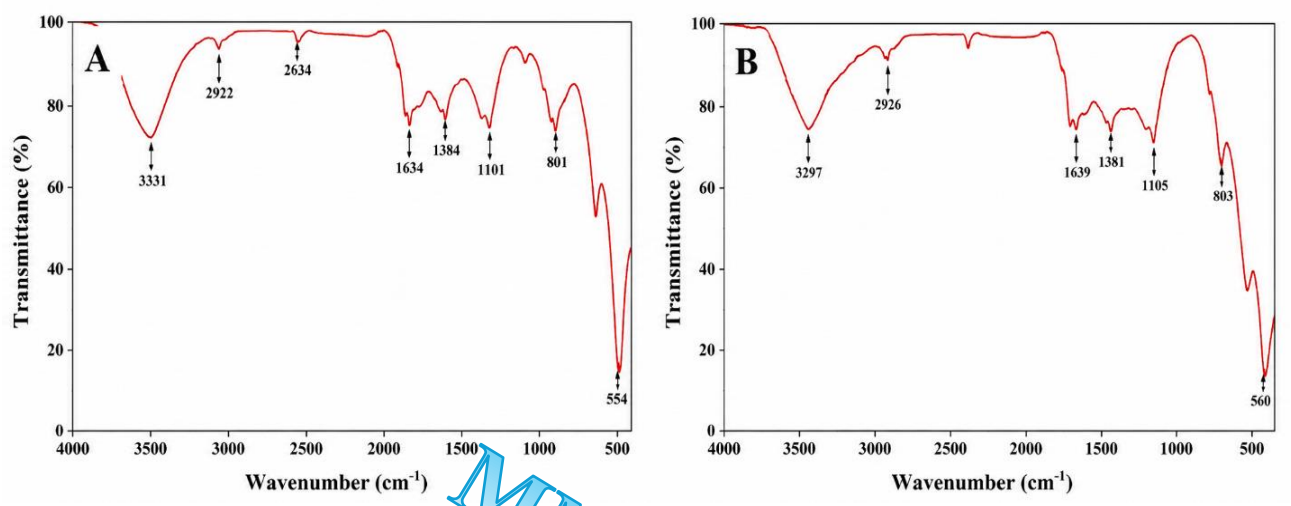


Figure 5. Fourier transform infrared (FTIR) spectra of Ni/NPs synthesized using (A) black tea extract (NiONPs-BT) and (B) green tea extract (NiONPs-GT). (**Note.** Characteristic peaks at 3200–3400 cm^{-1} (O–H stretching), 1630–1650 cm^{-1} (C=O and C=C), 1000–1100 cm^{-1} (C–O), and below 600 cm^{-1} (Ni–O) showed the presence of phytochemical functional groups involved in nanoparticle stabilization and capping.)

MMB In Press

The characteristic Ni–O stretching vibration was identified at wavenumbers below 600 cm^{-1}, confirming the formation of nickel oxide (Al-Shehri *et al.*, 2024; Bhosale *et al.*, 2025).

The presence of phytochemical-related functional groups in the FTIR spectra confirms that tea polyphenols participated in the reduction of Ni^{2+} ions and acted as capping agents, stabilizing the nanoparticles through surface adsorption. Similar findings have been reported for NiONPs synthesized using *C. sinensis* by Kalita *et al.* (2021) and *Azadirachta indica* by Karthik *et al.* (2022), both demonstrating the presence of phenolic and carbonyl groups on the nanoparticle surface. Surface functionalization with phytochemicals including flavonoids, catechins, tannins, phenolic acids, and flavones prevents excessive agglomeration during synthesis and enhances colloidal stability and biological activity (Mahmud & Rahman, 2025; Sati *et al.*, 2025). The broad O–H peak is more prominent in NiONPs-GT, possibly reflecting the higher content of catechins with multiple hydroxyl groups in green tea compared to the more polymerized polyphenols present in black tea (Kim *et al.*, 2017; Tahir *et al.*, 2024). These findings align with previous studies demonstrating that plant-mediated synthesis of NiONPs results in surface functionalization with bioactive phytochemicals, contributing to the enhanced antimicrobial properties of the nanoparticles (El-Kemary *et al.*, 2021; Uddin *et al.*, 2021).

3.5. Transmission electron microscopy (TEM) and scanning electron microscopy (SEM) analysis

The morphology and size of the biosynthesized NiONPs were examined using TEM and SEM (Figure 6). Both NiONPs-BT and NiONPs-GT exhibited predominantly quasi-spherical morphology with nanoscale dimensions. Quantitative analysis of TEM micrographs revealed average particle diameters of 33–38 nm for NiONPs-BT and 29–35 nm for NiONPs-GT, consistent with the UV-Vis blue shift and XRD crystallite size calculations (Sections 3.1 and 3.2). The larger size of NiONPs-BT suggests that black tea polyphenols provide more effective growth inhibition compared to green tea catechins, in agreement with previous reports (Rasheed & Jum'a, 2026; Tahir *et al.*, 2024). SEM images confirmed surface morphology and relatively uniform particle distribution with some agglomeration, which is typical for green-synthesized metal oxide nanoparticles (Hassan *et al.*, 2023; Sankar *et al.*, 2023).

The particle sizes measured by TEM (29–38 nm) were considerably smaller than the hydrodynamic diameters obtained by DLS (214.9–381.3 nm), as DLS measures the hydrated radius including capping layers and aggregates, while TEM measures the physical core diameter (Bhattacharjee *et al.*, 2016). The quasi-spherical morphology, which is widely reported for plant-mediated NiONPs, is associated with increased surface area and enhanced antimicrobial activity (Kaur, 2018). The observed aggregation, common for biosynthesized nanoparticles, does not compromise nanoscale structural stability, particularly given the excellent colloidal stability indicated by zeta potential measurements for NiONPs-BT (Sati *et al.*, 2025).

The ratio of DLS hydrodynamic diameter to TEM primary particle size provides an estimate of the average number of primary particles per agglomerate. For NiONPs-BT, the ratio (Z-average/TEM diameter) is approximately 214.9/35 ≈ 6.1, suggesting agglomerates containing, on average, approximately 6-7 primary particles. For NiONPs-GT, the ratio is approximately 381.3/32 ≈ 11.9, indicating larger agglomerates containing approximately 12 primary particles. This calculation assumes spherical agglomerates with a fractal dimension of 3 (dense packing), which may not fully represent the actual agglomerate structure but provides a useful comparative metric (Sorensen, 2001; Bhattacharjee *et al.*, 2016).

The bimodal size distribution observed for both formulations indicates the coexistence of small agglomerates (58.1-163.2 nm, representing 2-5 primary particles) and larger agglomerates (303.3-1449.4 nm, representing 9-45 primary particles).

The presence of these larger agglomerates dominates the Z-average and explains the high PDI values. Notably, NiONPs-GT shows a more pronounced large-agglomerate peak (1449.4 nm) compared to NiONPs-BT (303.3 nm), consistent with its less negative zeta potential and consequently weaker electrostatic stabilization.

The significantly more negative zeta potential of NiONPs-BT (-44.4 mV vs. -20.7 mV for NiONPs-GT) explains its superior colloidal stability and smaller agglomerate size despite both formulations having similar primary particle sizes. Zeta potential magnitudes above ±30 mV are generally considered sufficient for electrostatic stabilization, whereas values below ±30 mV indicate a propensity for agglomeration (Bhattacharjee *et al.*, 2016; Zheng *et al.*, 2011). The -44.4 mV value for NiONPs-BT provides strong electrostatic repulsion between particles, limiting agglomeration, whereas the -20.7 mV value for NiONPs-GT offers only moderate stabilization, allowing more extensive agglomeration. This difference in surface charge likely reflects the distinct phytochemical composition of the capping layers: black tea polyphenols (theaflavins/thearubigins) may provide more effective surface coverage and a higher density of ionizable hydroxyl groups compared to green tea catechins, resulting in a more negative surface charge (Rasheed & Jum'a, 2026; Tahir *et al.*, 2024; Zheng *et al.*, 2011).

3.6. Minimum inhibitory concentration (MIC) and minimum bactericidal concentration (MBC) determination

The antibacterial activity of NiONPs-BT and NiONPs-GT was quantitatively evaluated against *S. aureus*, *E. coli*, and *L. monocytogenes* using the broth microdilution method (Figure 7 and Table 2). NiONPs-BT consistently showed lower MIC and MBC values than NiONPs-GT across all tested strains, with the highest susceptibility observed for *L. monocytogenes*, followed by *S. aureus* and *E. coli*.

The highest susceptibility was observed for *L. monocytogenes*, followed by *S. aureus* and *E. coli*. For *S. aureus*, the MBC/MIC values were 50/25 µg/mL for NiONPs-BT and 100/50µg/mL for NiONPs-GT. For *E. coli*, NiONPs-BT showed MIC and MBC values of 50 and 100 µg/mL, respectively, whereas the MIC of NiONPs-GT was 100 µg/mL and its MBC was >100 µg/mL. *L. monocytogenes* was the most susceptible strain, with MBC/MIC values of 25/12.5 µg/mL for NiONPs-BT and 50/25µg/mL for NiONPs-GT. The MBC/MIC ratio was 2 for all combinations with measurable MBC values, indicating a bactericidal effect according to the predefined criterion (MBC/MIC ≤4). For NiONPs-GT against E. coli, the MBC/MIC ratio was 1.25, which also falls within the bactericidal range (MBC/MIC ≤ 4). Thus, all nanoparticle–strain combinations for which MBC values were determined exhibited bactericidal activity; no bacteriostatic effect (MBC/MIC > 4) was observed under the assay conditions.

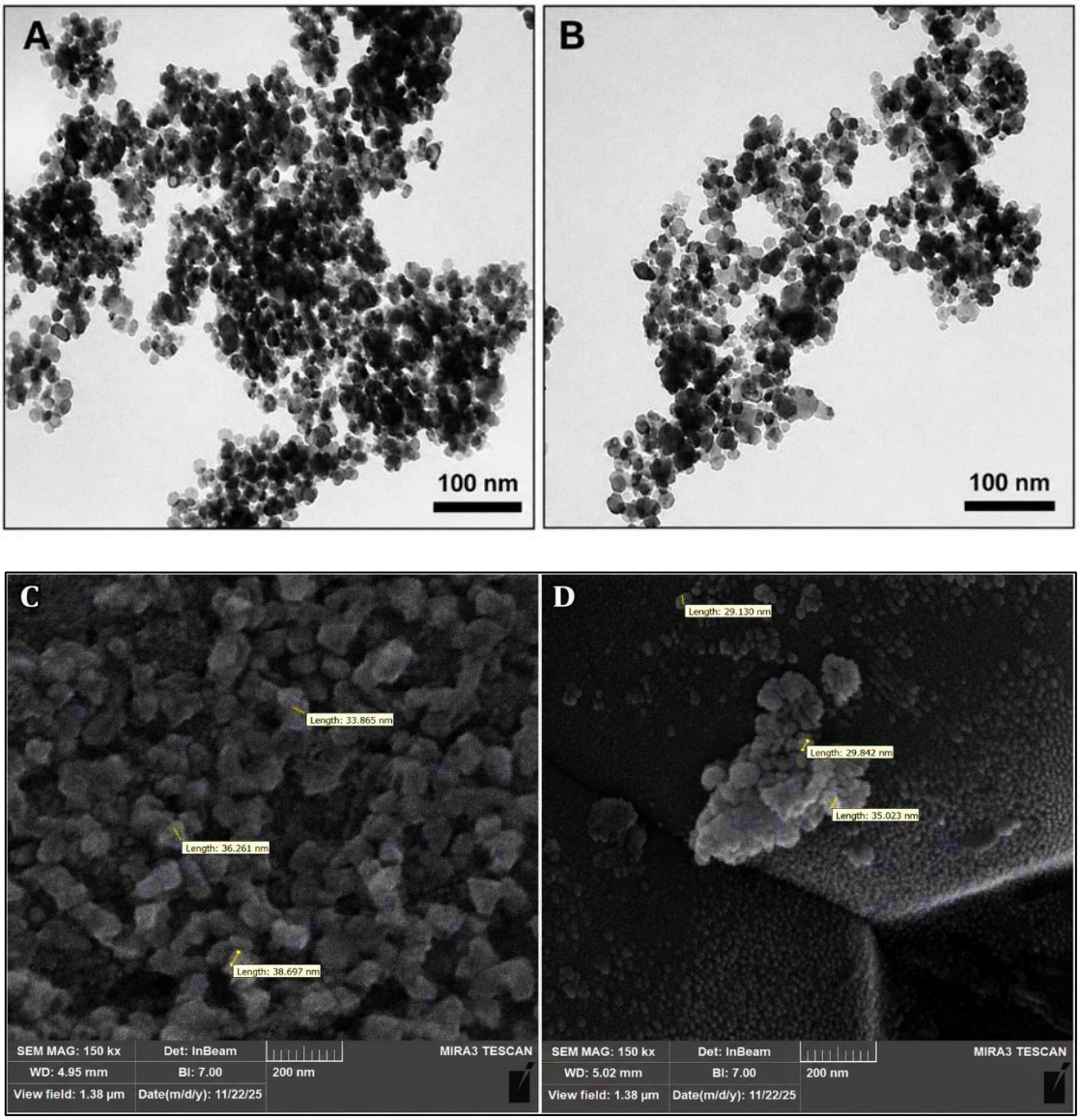


Figure 6. TEM and SEM micrographs images of NiONPs-BT (A and C) and NiONPs-GT (B and D) nanoparticles. (**Note.** TEM analysis revealed quasi-spherical morphology with mean diameters of 33–38 nm for (NiONPs-BT) and 29–35 nm for (NiONPs-GT). Scale bars: 200 nm.)

Table 2. MIC and MBC of NiONPs-BT, NiONPs-GT, and $NiCl_2$ against Selected Bacteria

Bacterial Strain	Compound	MIC (µg/mL)	MBC (µg/mL)	MBC/MIC	Effect
S. aureus	NiONPs-BT	25	50	2	Bactericidal
	NiONPs-GT	50	100	2	Bactericidal
	$NiCl_2$	25	50	2	Bactericidal
E. coli	NiONPs-BT	50	100	2	Bactericidal
	NiONPs-GT	100	125	1.25	Bactericidal
	$NiCl_2$	100	125	1.25	Bactericidal
L. monocytogenes	NiONPs-BT	12.5	25	2	Bactericidal
	NiONPs-GT	25	50	2	Bactericidal
	$NiCl_2$	12.5	25	2	Bactericidal

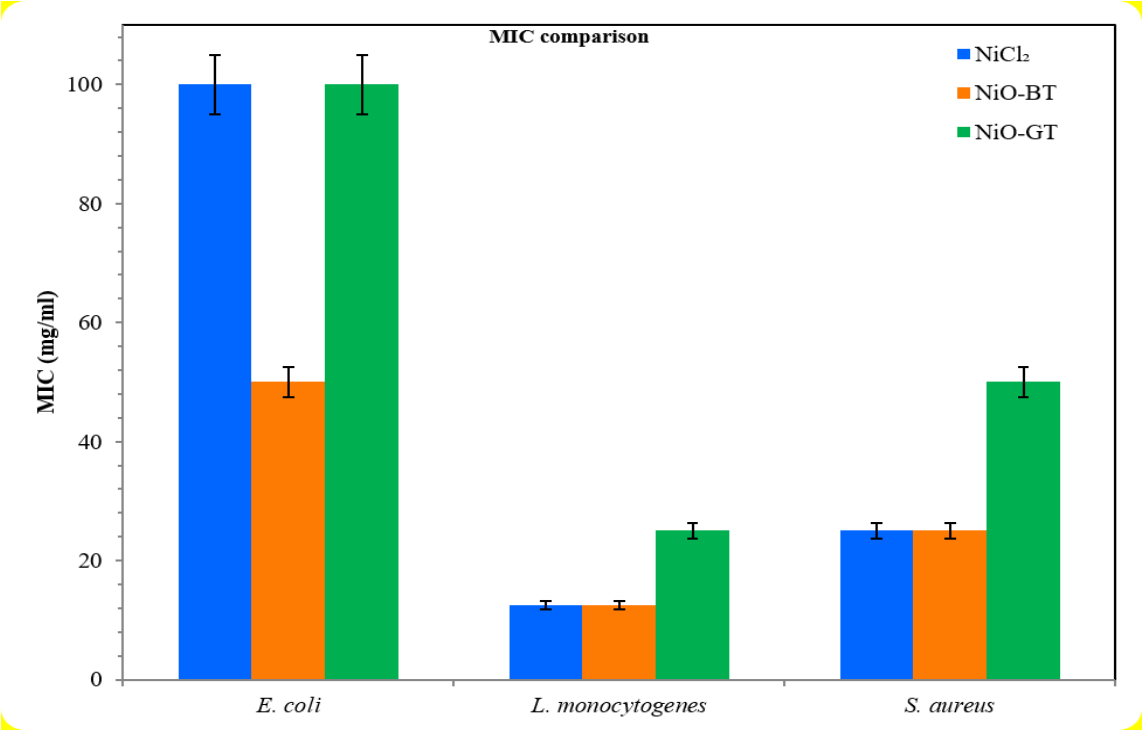


Figure 7. Minimum inhibitory concentration (MIC) of NiONPs-BT, NiONPs-GT, and $NiCl_2$ against *S. aureus*, *E. coli*, and *L. monocytogenes*. (**Note.** Data represent mean values from three independent experiments. NiONPs-BT exhibited the lowest MIC values across all strains, demonstrating superior antibacterial activity compared to NiONPs-GT, with performance comparable to or better than the $NiCl_2$ precursor.)

The greater activity of NiONPs-BT may be related to differences in the physicochemical properties of the two nanoparticle preparations, including their surface characteristics and phytochemical capping layers. In particular, the more negative zeta potential observed for NiONPs-BT (−44.4 mV vs. −21.7 mV) may contribute to differences in colloidal stability and nanoparticle–cell interactions. However, this proposed mechanism is correlative and requires further investigation. The greater susceptibility of *L. monocytogenes* and *S. aureus* compared with *E. coli* is also consistent with the generally higher sensitivity of Gram-positive bacteria to metal oxide nanoparticles, although bacterial susceptibility can vary with cell-envelope structure and nanoparticle characteristics (Almatroudi, 2020; Slavin *et al.*, 2017). Overall, NiONPs-BT exhibited greater antibacterial potency than NiONPs-GT, with the strongest activity observed against *L. monocytogenes*.

MBC/MIC ratios ≤4 indicate bactericidal activity, while ratios >4 indicate bacteriostatic activity (Pankey & Sabath, 2004). The superior activity of NiONPs-BT compared to NiONPs-GT across all strains is evident, with NiONPs-BT showing equivalent or better activity than the $NiCl_2$ precursor. Also, NiONPs-GT against *E. coli* exhibited bactericidal behavior (MBC/MIC ≤ 4); NiONPs-BT, NiONPs-GT, and $NiCl_2$ all showed bactericidal activities against selected strains.

The MIC values observed in this study are comparable to those reported for other metal oxide nanoparticles against foodborne pathogens. For example, ZnO nanoparticles have been reported to exhibit MIC values of 25-100 µg/mL against *S. aureus* and *E. coli* (Raghupathi *et al.*, 2011; Sirelkhatim *et al.*, 2015), while CuO nanoparticles showed MIC values of 50-200 µg/mL against similar strains (Ren *et al.*, 2009; Azam *et al.*, 2012). The NiONPs-BT formulation, with MIC values as low as 12.5 µg/mL against *L. monocytogenes*, demonstrates comparable or superior activity to these previously reported metal oxide nanoparticles (Azam *et al.*, 2012; Raghupathi *et al.*, 2011; Ren *et al.*, 2009; Sirelkhatim *et al.*, 2015).

3.7. Sub-MIC selection and antibiofilm activity

The antibiofilm activity of NiONPs-BT and NiONPs-GT was evaluated at sub-inhibitory concentrations (¼ MIC and ½ MIC) against *S. aureus*, *E. coli*, and *L. monocytogenes* using the crystal violet staining method (Figure 8).

Both formulations exhibited concentration-dependent biofilm inhibition across all strains, with NiONPs-BT consistently demonstrating superior activity. For *S. aureus*, NiONPs-BT inhibited biofilm formation by 39.5%, 64.9%, and 88.6% at ¼ MIC (6.25 µg/mL), ½ MIC (12.5 µg/mL), and MIC (25 µg/mL), respectively, compared to 21.6%, 48.6%, and 79.5% inhibition by NiONPs-GT at corresponding equal concentrations. Against *E. coli*, NiONPs-BT showed 22.4%, 46.1%, and 81.2% inhibition at ¼ MIC (12.5 µg/mL), ½ MIC (25 µg/mL), and MIC (50 µg/mL), while NiONPs-GT exhibited 13.9%, 30.3%, and 68.5% inhibition at equal concentrations, respectively. The most pronounced activity was observed against *L. monocytogenes*, where NiONPs-BT achieved 58.5%, 78.5%, and 92.3% inhibition at ¼ MIC (3.125 µg/mL), ½ MIC (6.25 µg/mL), and MIC (12.5 µg/mL), compared to 42.6%, 65.1%, and 87.2% inhibition by NiONPs-GT at equal concentrations, respectively.

MMB In Press

The superior antibiofilm efficacy of NiONPs-BT is attributed to its enhanced colloidal stability and more negative surface charge (-44.4 mV vs. -20.7 mV), which facilitate stronger electrostatic interactions with bacterial cell surfaces and biofilm matrix components (Bhattacharjee *et al.*, 2016; Khan *et al.*, 2022). The order of bacterial susceptibility corresponded with the MIC results: *L. monocytogenes* > *S. aureus* > *E. coli*, reflecting the inherent structural differences between Gram-positive and Gram-negative bacteria (Almatroudi, 2020; Slavin *et al.*, 2017). A key finding was the significant antibiofilm activity observed at sub-MIC concentrations, where minimal effects on planktonic growth were noted. This suggests that NiONPs-BT and NiONPs-GT inhibit biofilm formation by targeting EPS production, adhesion, and biofilm maturation rather than through direct growth inhibition (Ferreres *et al.*, 2023; Naskar & Kim, 2019). However, this proposed mechanism is inferred from the sub-MIC activity and requires direct confirmation through, for example, EPS quantification or adhesion assays. The enhanced activity of NiONPs-BT compared to $NiCl_2$ (e.g., 81.2% vs. 58.8% inhibition against *E. coli* at MIC) showed that green synthesis using black tea extract produces nanoparticles with superior antibiofilm properties beyond simple ionic toxicity, likely due to a synergistic "nano-effect" and localized reactive oxygen species (ROS) production (Singh *et al.*, 2018; Yaqoob *et al.*, 2020). The contribution of ROS to the observed antibiofilm effects remains to be directly measured.

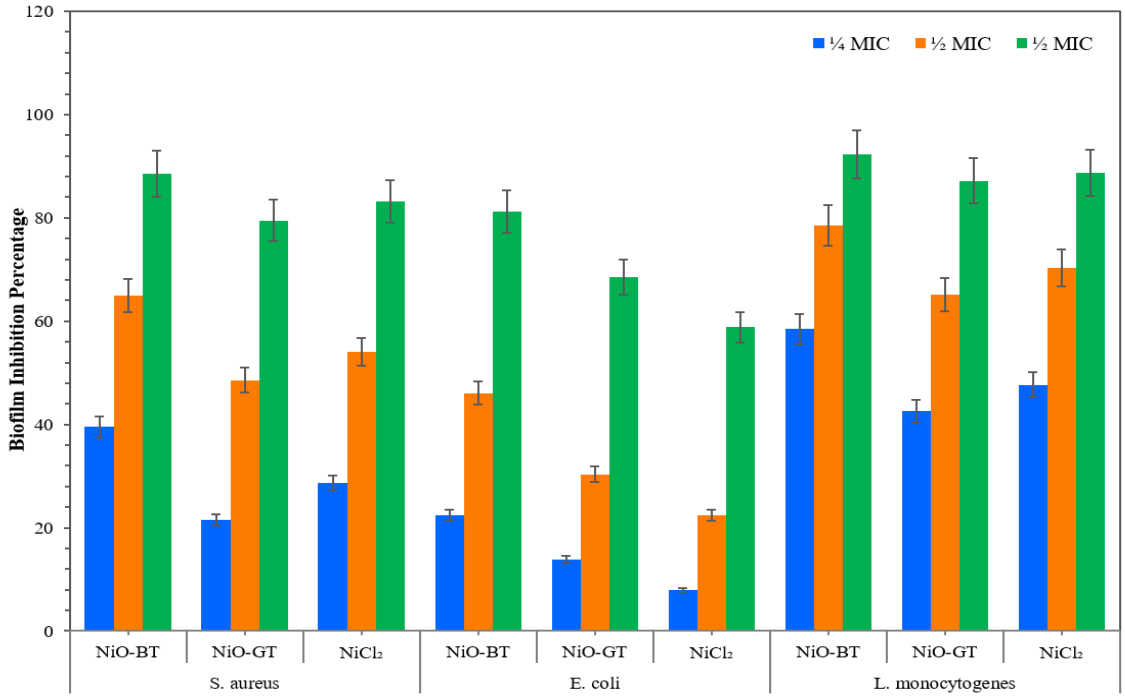


Figure 8. Biofilm inhibition percentages of *S. aureus, E. coli, and L. monocytogenes* following treatment with sub-MIC and MIC concentrations of NiONPs-BT and NiONPs-GT. (**Note.** Data represent mean ± SD (n=3). NiONPs-BT consistently exhibited superior antibiofilm activity across all strains and concentrations.)

3.8. Molecular analysis of biofilm- and quorum sensing-associated genes

To elucidate the molecular mechanisms underlying the antibiofilm activity of NiONPs, the expression of selected biofilm- and quorum sensing-related genes was assessed by quantitative real-time PCR following treatment with sub-inhibitory concentrations (½ MIC) of NiONPs-BT and NiONPs-GT. The results of relative gene expression calculated using the $2^{-\Delta\Delta Ct}$ method with 16S rRNA serving as the internal reference and melting curves are shown in Table 3 and Figures 9 and 10, respectively. Also, the relative expression of biofilm- and quorum sensing-associated genes in *S. aureus*, *E. coli*, and *L. monocytogenes* are shown in Figure 11. Treatment with both nanoparticle formulations resulted in significant downregulation of all tested genes across the three bacterial species ($P < 0.05$–0.001), with NiONPs-BT consistently inducing stronger transcriptional suppression than NiONPs-GT.

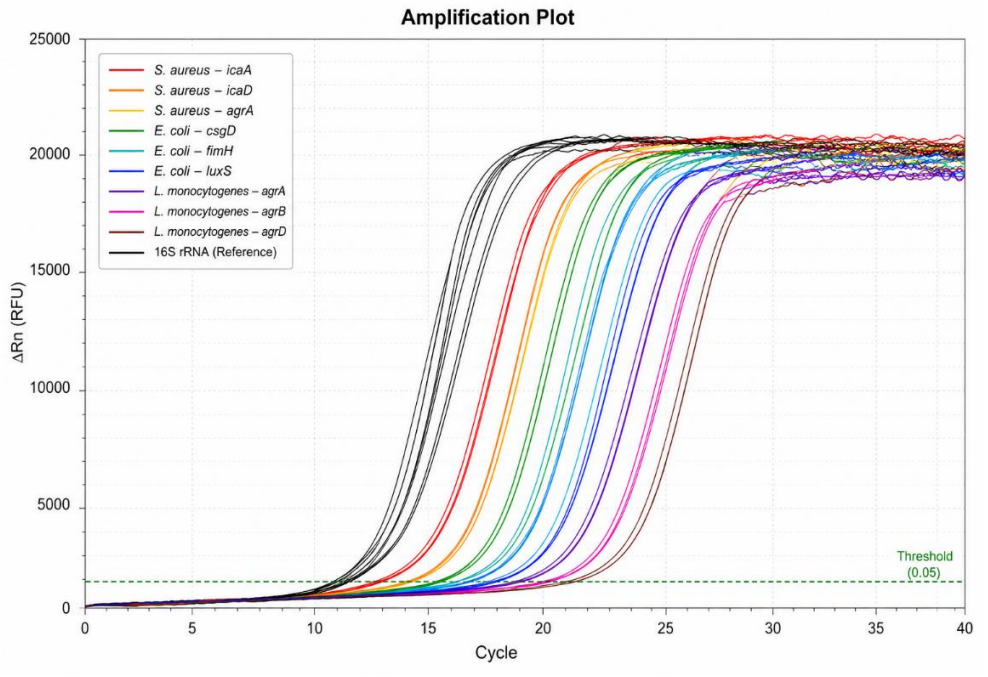


Figure 9. qPCR amplification curves. Representative real-time PCR amplification curves for biofilm- and quorum sensing-associated genes in *S. aureus*, *E. coli*, and *L. monocytogenes* following treatment with sub-inhibitory concentrations (½ MIC) of NiONPs-BT and NiONPs-GT nanoparticles. (**Note.** The curves show the increase in fluorescence (ΔRn) as a function of amplification cycle. Each assay was performed in biological triplicate (n = 3).)

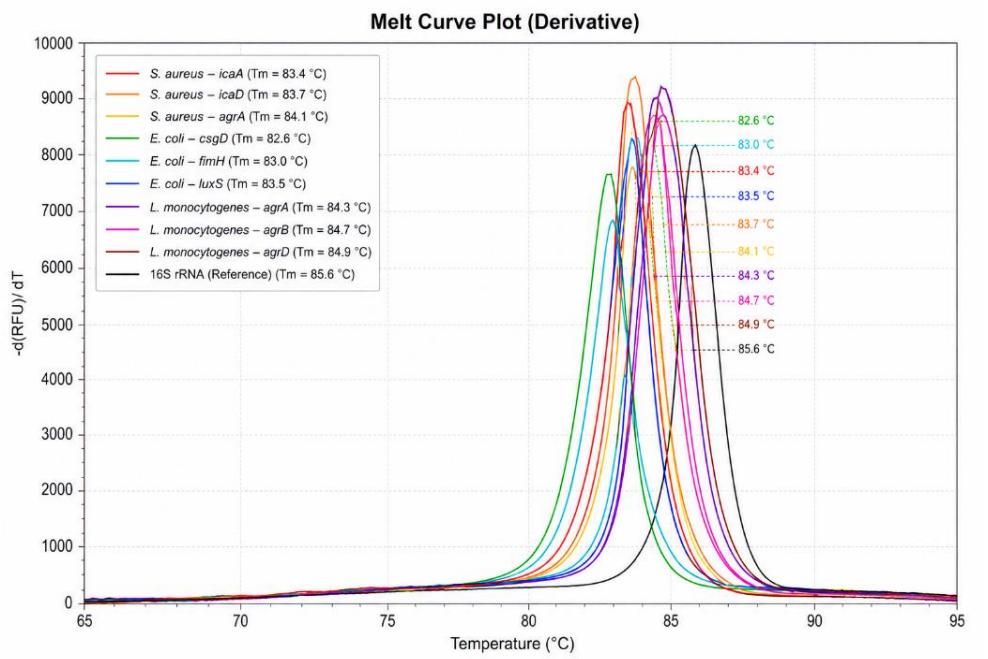


Figure 10. qPCR melting-curve analysis. Derivative melting curves [−d(RFU)/dT] of PCR products corresponding to biofilm- and quorum sensing-associated genes in *S. aureus*, *E. coli*, and *L. monocytogenes*. (**Note.** The 16S rRNA amplicon was included as the internal reference.)

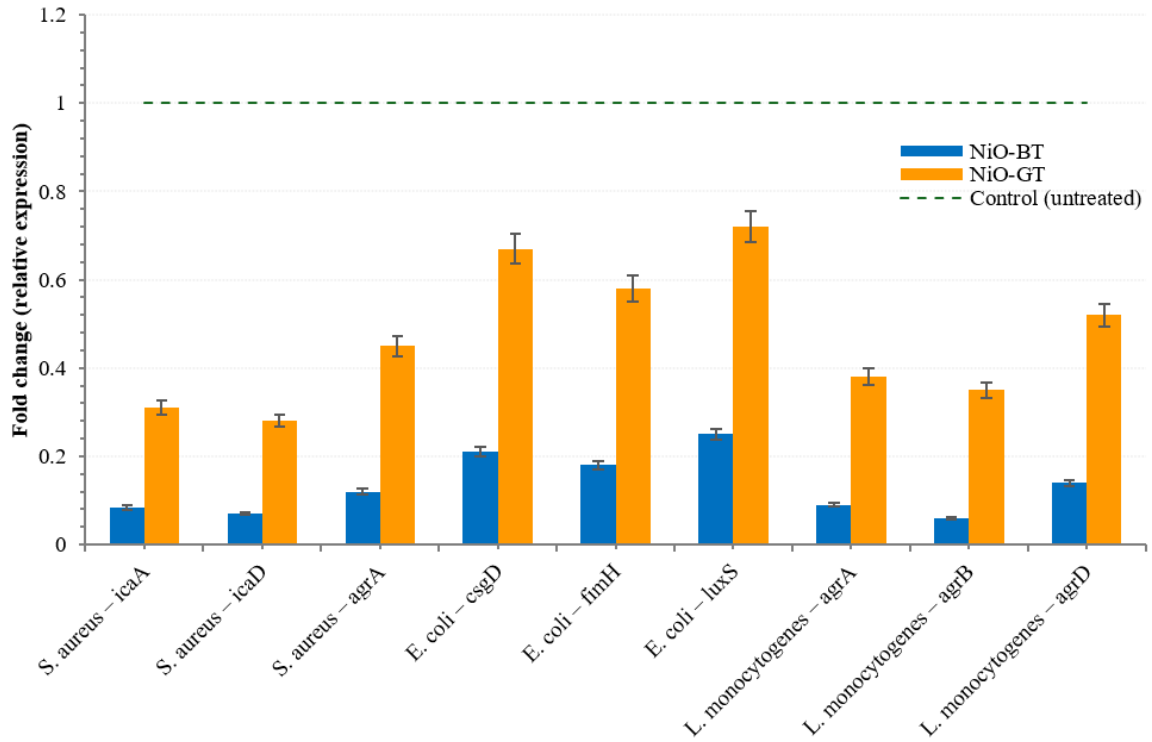


Figure 11. Relative Expression of Biofilm- and Quorum Sensing-associated Genes in *S. aureus*, *E. coli*, and *L. monocytogenes* following Treatment with ½ MIC of NiONPs-BT and NiONPs-GT Nanoparticles. Data are presented as fold change relative to untreated controls (mean ± SD, n=3). NiONPs-BT induced significantly stronger transcriptional suppression than NiONPs-GT across all tested genes ($P < 0.05–0.001$).

Table 3. Relative Gene Expression (Fold Change) of Biofilm- and Quorum Sensing-Associated Genes Following Treatment with ½ MIC of NiONPs-BT and NiONPs-GT

Strain	Gene	Function	Fold Change (NiONPs-BT)	Fold Change (NiONPs-GT)	p-value
S. aureus	*icaA*	PIA/PNAG biosynthesis	0.084	0.31	<0.01
	icaD		0.071	0.28	<0.01
	agrA	Quorum sensing	0.12	0.45	<0.001
E. coli	*csgD*	Curli master regulator	0.21	0.67	<0.001
	fimH	Type 1 fimbrial adhesin	0.18	0.58	<0.001
	luxS	Quorum sensing (AI-2)	0.25	0.72	<0.001
L. monocytogenes	*agrA*	Quorum sensing	0.09	0.38	<0.01
	agrB		0.06	0.35	<0.01
	agrD		0.14	0.52	<0.01

Note. Data represent fold change relative to untreated controls (normalized to 1.0). Values <1 indicate downregulation; lower values indicate stronger suppression. All *p*-values were calculated using Student's t-test (n=3).

3.8.1. Staphylococcus aureus

In *S. aureus*, NiONPs-BT treatment reduced the expression of *icaA*, *icaD*, and *agrA* by 0.084-, 0.071-, and 0.12-fold, respectively, whereas NiONPs-GT caused milder reductions of 0.31-, 0.28-, and 0.45-fold. The *icaAD* operon encodes polysaccharide intercellular adhesin (PIA), a key component of the extracellular polymeric matrix essential for biofilm accumulation and stability (Arciola *et al.*, 2015; Greco *et al.*, 2008). The agr system, a two-component QS regulatory cascade, controls virulence factor production and biofilm dynamics. The concurrent downregulation of both adhesion (PIA) and regulatory (Agr) pathways likely explains the pronounced reduction in biofilm formation observed in the crystal violet assays (Section 3.8). However, it should be noted that the Agr system is a QS regulatory cascade, and reduced agr expression does not necessarily indicate direct quorum quenching; it may reflect indirect effects of nanoparticle exposure on global transcriptional regulators or stress responses. Previous studies on silver (Ag) and zinc oxide (ZnO) nanoparticles have similarly reported transcriptional suppression of *icaA* and *agrA* genes in *S. aureus* biofilms (Abdulsattar *et al.*, 2026; Gheidar *et al.*, 2018), supporting the role of metal oxide nanoparticles in modulating the expression of QS-associated genes.

3.8.2. Escherichia coli

In *E. coli*, NiONPs-BT suppressed the expression of *csgD* (0.21-fold), *fimH* (0.18-fold), and *luxS* (0.25-fold), whereas NiONPs-GT caused reductions of 0.67-, 0.58-,

and 0.72-fold, respectively. *csgD* is the master regulator of curli fimbriae and cellulose biosynthesis, which are essential for initial adhesion and biofilm maturation. *fimH* is a type 1 fimbrial adhesin that mediates host tissue invasion and biofilm adherence. *luxS* catalyzes the synthesis of autoinducer-2 (AI-2), a key signaling molecule involved in interspecies QS communication. The concurrent inhibition of these interconnected pathways suggests that NiONPs disrupt multiple stages of biofilm development, from initial adhesion (mediated by *fimH*) to maturation (regulated by *csgD*-controlled curli and cellulose) and QS-mediated coordination (via *luxS*/AI-2). However, direct quorum-quenching activity was not assessed, and the observed effects may be indirect. This multi-targeted suppression parallels previous findings for silver (Ag) and zinc oxide (ZnO) nanoparticles against *E. coli* biofilms (Niu *et al.*, 2013).

MMB In Press

3.8.3. Listeria monocytogenes

In *L. monocytogenes*, NiONPs-BT reduced the expression of *agrA* (0.09-fold), *agrB* (0.06-fold), and *agrD* (0.14-fold), while NiONPs-GT caused reductions of 0.38-, 0.35-, and 0.52-fold, respectively. The *agr* operon in *L. monocytogenes* is a key virulence regulator that controls biofilm formation, environmental adaptability, and immune evasion (Duru *et al.*, 2021; Rieu *et al.*, 2007). The significant suppression of agr expression correlates with the strong antibiofilm activity observed against this strain (Section 3.8). Recent studies have demonstrated that interference with the *Agr* signaling pathway represents a promising anti-virulence strategy against *L. monocytogenes* infections (Shao *et al.*, 2026; Zhang *et al.*, 2022). The stronger suppression induced by NiONPs-BT compared to NiONPs-GT suggests that the phytochemical composition of black tea extract enhances nanoparticle-mediated suppression of QS-associated gene expression. However, this does not constitute direct evidence of quorum quenching, and further studies are required to determine whether NiONPs directly interfere with QS signaling mechanisms.

The superior gene suppression capacity of NiONPs-BT across all tested strains corresponds with its enhanced colloidal stability and more negative surface charge (-44.4 mV vs. -20.7 mV), which likely facilitates more efficient cellular interactions and internalization (Bhattacharjee *et al.*, 2016). However, direct evidence of internalization or specific molecular interactions was not obtained. The genes examined, *icaA*, *icaD*, *agrA*/*B*/*D*, *csgD*, *fimH*, and *luxS* represent core components of the QS and biofilm regulatory networks in both Gram-positive and Gram-negative bacteria. Simultaneous targeting of these interconnected pathways may yield more pronounced anti-virulence effects than interfering with a single regulatory cascade, as demonstrated in recent studies on combined targeting of virulence factors in biofilm-associated infections (Afrasiabi *et al.*, 2025). Overall, the molecular data demonstrate that tea-synthesized NiONPs, particularly NiONPs-BT, suppress the expression of QS-associated and biofilm-related genes at the transcriptional level.

While these findings suggest interference with QS regulatory networks, direct quorum-quenching activity (e.g., signal molecule degradation or receptor antagonism) was not assessed in this study. These findings align with previous reports on biogenic ZnO and Se nanoparticles (Nowak *et al.*, 2026) and underscore the potential of NiONPs-BT as a sustainable anti-virulence agent for food safety applications. The comparative analysis of black and green tea-mediated synthesis provides a foundation for future research on the influence of phytochemical composition on the bactericidal and antibiofilm properties of metal oxide nanoparticles.

3.9. Limitations in this study

A limitation of this study is the absence of extract-only controls in the antibacterial and antibiofilm assays. Tea extracts contain high concentrations of bioactive polyphenols, including catechins, theaflavins, and thearubigins, which possess intrinsic antibacterial and antibiofilm properties. Consequently, the possibility that residual extract-derived phytochemicals associated with the nanoparticle surface contribute to the observed biological activities cannot be excluded. While the superior activity of NiONPs-BT compared to NiONPs-GT and the Ni^{2+} precursor suggests a nanoparticle-specific effect, the precise contribution of the organic capping layer versus the inorganic NiO core to the overall antibacterial and antibiofilm activity remains to be fully elucidated. Future studies should include extract-only controls at equivalent concentrations to definitively attribute the observed effects to the nanoparticles themselves. Also, the organic content of the calcined NiONPs was not quantified in this study.

In FTIR analysis, the presence of residual organic functional groups and the possibility that the observed differences between NiONPs-BT and NiONPs-GT arise from differences in inorganic surface properties (e.g., defect density, surface hydroxylation) rather than organic capping cannot be excluded. Thermogravimetric and elemental analysis are recommended in future work to quantify the organic content and better understand its role in the physicochemical and biological properties of the nanoparticles.

4. Conclusion

This study demonstrated that NiONPs green-synthesized using black and green tea extracts exhibit potent antibacterial and antibiofilm activities against *S. aureus*, *E. coli*, and *L. monocytogenes*, and suppress the expression of QS-associated and biofilm-related genes. However, direct quorum-quenching activity was not assessed, and the observed transcriptional effects may involve indirect mechanisms. Physicochemical characterization revealed that NiONPs-BT possessed superior colloidal stability (−44.4 mV) and larger crystallite sizes (31.3 nm) compared to NiONPs-GT (−20.7 mV; 29.8 nm), correlating with enhanced antibacterial performance. The MIC and MBC assays showed bactericidal activity for NiONPs-BT against all tested strains (MBC/MIC $\leq$ 4), whereas NiONPs-GT exhibited bacteriostatic effects against *E. coli* (MBC/MIC $>$ 2). Notably, both formulations significantly inhibited biofilm formation at sub-MIC concentrations, with

NiONPs-BT achieving up to 92.3% inhibition against *L. monocytogenes* at MIC. Quantitative real-time PCR analysis revealed that NiONPs-BT induced stronger transcriptional suppression of key biofilm- and QS-associated genes, including *icaA* (0.084-fold), csgD (0.21-fold), and agrB (0.06-fold), providing molecular insight into the observed anti-virulence activity. However, these findings do not confirm direct quorum-quenching activity, and future studies should include direct signal-interference assays to validate this mechanism.

The superior efficacy of NiONPs-BT is attributed to the synergistic combination of the nano-effect and ionic toxicity, enhanced by the phytochemical composition of black tea extract. These findings position tea-mediated NiONPs, particularly NiONPs-BT, as promising sustainable anti-virulence and antibiofilm agents for food preservation applications. This study is limited to in vitro screening, and further studies are necessary to evaluate their efficacy in complex food matrices, long-term stability, and potential for resistance development, as well as to elucidate the precise mechanisms by which tea phytochemicals influence nanoparticle properties and biological activity, including whether they possess direct quorum-quenching activity.

The comparative approach employed in this study provides a foundation for optimizing green synthesis strategies to develop next-generation antimicrobial nanomaterials. However, it must be emphasized that the transformation of these findings to food-safety applications requires careful consideration of potential toxicity, residual nickel release, environmental fate, and regulatory compliance. The known sensitizing and carcinogenic potential of nickel, combined with the absence of comprehensive toxicity and migration data for NiONPs in food-contact scenarios, necessitates a precautionary approach. Future studies must prioritize biocompatibility assessment, migration testing under realistic conditions, and environmental safety evaluation before any practical application can be responsibly proposed. Also, the evaluation of efficacy in complex food matrices, long-term stability, and potential for resistance development and the precise mechanisms by which tea phytochemicals influence nanoparticle properties should be considered. Also, comprehensive toxicity assessments (e.g., MTT, LDH, and ROS assays on relevant mammalian cell lines) should be considered. The development of safer formulations (e.g., surface-modified or encapsulated NiONPs with reduced nickel release) may offer a pathway toward balancing antimicrobial efficacy with safety.

Conflict of interest

The authors declare no conflict of interest.

Acknowledgment

The author would like to thank the Vice President for Research and Technology at the Lahijan Branch, Islamic Azad University, Lahijan, Iran, for providing the facilities.

Ethical approval

This article does not contain any studies with human participants or animals performed by any of the authors.

Open access

This article is distributed under the terms of the Creative Commons Attribution License which permits unrestricted use, distribution, and reproduction in any medium, provided the original work is properly cited.

Funding

None declared.

Authors' Contributions

Maryam Basbus : Methodology, Investigation, Formal analysis, Writing original draft of the manuscript. Mirsasan Mirpour and Mohammad Faezi Ghasemi: Writing – review & editing, Validation, Supervision, Project administration, Conceptualization. Behnam Rasti Resources, Visualization. All authors have read and approved the final version of the manuscript.

References

Abdulsattar, B. O., Abdulsattar, J. O., Abdulmunem, O. M., Abbas, B. F., Neif, O. A., & Mohammad, M. A. (2026). Down-regulation of biofilm formation genes expression on some gram-negative bacteria by Fumaria officinalis extract. *Journal of microbiological methods*, 107472.

Afrasiabi, S., Partoazar, A., Goudarzi, R., & Dehpour, A. R. (2025). Carbon-Based Nanomaterials Alter the Behavior and Gene Expression Patterns of Bacteria. *Journal of basic microbiology*, *65*(5), e2400545.

Al-Shehri, S., Alshehri, S., Ali, H. E., Ibrahim, E. H., Alzahrani, A. O. M., Abdel-Daim, A., Alassafi, J. E., & Aida, M. (2024). Synthesis of multifunctional flexible polymeric PVA/PEG blend nanocomposite films filled with AZO nanoparticles. *Polymer Bulletin*, *81*(16), 14561–14585.

Alavi, M., Pedro, S. N., Freire, M. G., Ashengroph, M., & Khan, H. (2025). Theaflavins applications to ameliorate implant failure and eradicate microbial infections and foodborne pathogens: a comprehensive review. *Phytotherapy Research*, *39*(1), 494–504.

Almatroudi, A. (2020). Silver nanoparticles: synthesis, characterisation and biomedical applications. *Open life sciences*, *15*(1), 819–839.

Arciola, C. R., Campoccia, D., Ravaioli, S., & Montanaro, L. (2015). Polysaccharide intercellular adhesin in biofilm: structural and regulatory aspects. *Frontiers in cellular and infection microbiology*, *5*, 7.

Azam, A., Ahmed, A. S., Oves, M., Khan, M. S., Habib, S. S., & Memic, A. (2012). Antimicrobial activity of metal oxide nanoparticles against Gram-positive and Gram-negative bacteria: a comparative study. *International journal of nanomedicine*, 6003–6009.

Balouiri, M., Sadiki, M., & Ibnsouda, S. K. (2016). Methods for in vitro evaluating antimicrobial activity: A review. *Journal of pharmaceutical analysis*, *6*(2), 71–79.

Bhattacharjee, S., Ray, A., Samanta, A., Das, S. N., Mukhopadhyay, A. K., & Ghosh, C. K. (2019). Electron–Phonon interaction to tune pseudocapacitive

properties of NiO. *Physica B: Condensed Matter*, *575*, 411686.

Bhattacharjee, S., Sarkar, B., Ranjan Sharma, A., Gupta, P., Sharma, G., Lee, S.-S., & Chakraborty, C. (2016). Formulation and application of biodegradable nanoparticles based biopharmaceutical delivery-an efficient delivery system. *Current Pharmaceutical Design*, *22*(20), 3020–3033.

Bhosale, M., Morankar, P. J., Amate, R. U., & Jeon, C.-W. (2025). Rational Designing of NiO Nanoparticles Anchored with PEG-WO3 for Enhanced Water Oxidation Performance. *Polymers*, *17*(9), 1281.

Bilici, Z., Koc, E., Özdemir, S., Yalçın, M., Filiz, V., & Dizge, N. (2025). Green synthesis of nickel oxide nanoflowers from cherry straw extract and preparation of antibacterial PES ultrafiltration membrane. *International Journal of Environmental Science and Technology*, *22*(14), 14245–14262.

Boban, T., Nadar, S., & Tauro, S. (2023). Breaking down bacterial communication: a review of quorum quenching agents. *Future Journal of Pharmaceutical Sciences*, *9*(1), 77.

Brand-Williams, W., Cuvelier, M.-E., & Berset, C. (1995). Use of a free radical method to evaluate antioxidant activity. *LWT-Food science and Technology*, *28*(1), 25–30.

Bustin, S. A., Benes, V., Garson, J. A., Hellemans, J., Huggett, J., Kubista, M., Mueller, R., Nolan, T., Pfaffl, M. W., & Shipley, G. L. (2009). The MIQE Guidelines: M inimum I nformation for Publication of Q uantitative Real-Time PCR E xperiments. In: Oxford University Press.

Cao, Z., Pan, Z., & Chen, Z. (2025). A comparative study on in-situ synthesis of two iron nanoparticles in acid mine drainage using green tea and Excoecaria cochinchinensis leaves extracts. *Chemosphere*, *381*, 144488.

Dsouza, F. P., Dinesh, S., & Sharma, S. (2024). Understanding the intricacies of microbial biofilm formation and its endurance in chronic infections: a key to advancing biofilm-targeted therapeutic strategies. *Archives of Microbiology*, *206*(2), 85.

Duru, I. C., Bucur, F. I., Andreevskaya, M., Nikparvar, B., Ylinen, A., Grigore-Gurgu, L., Rode, T. M., Crauwels, P., Laine, P., & Paulin, L. (2021). High-pressure processing-induced transcriptome response during recovery of Listeria monocytogenes. *BMC genomics*, *22*(1), 117.

El-Kemary, B. M., El-Borady, O. M., Abdel Gaber, S. A., & Beltagy, T. M. (2021). Role of nano-zirconia in the mechanical properties improvement of resin cement used for tooth fragment reattachment. *Polymer Composites*, *42*(7), 3307–3319.

Elmegdar, S., Elkheloui, R., Laktib, A., Mimouni, R., & Hamadi, F. (2024). Antibiofilm and anti-quorum sensing activities of biological nanoparticles. *Current Applied Science and Technology*, e0257479–e0257479.

Ferreres, G., Ivanova, K., Ivanov, I., & Tzanov, T. (2023). Nanomaterials and coatings for managing antibiotic-resistant biofilms. *Antibiotics*, *12*(2), 310.

Flentie, K., Spears, B. R., Chen, F., Purmort, N. B., DaPonte, K., Viveiros, E., Phelan, N., Krebill, C., Flyer, A. N., & Hooper, D. C. (2019). Microplate-based surface area assay for rapid phenotypic antibiotic susceptibility testing. *Scientific Reports*, *9*(1), 237.

Gheidar, H., Haddadi, A., Kalani, B. S., & Amirmozafari, N. (2018). Nanoparticles impact the expression of the genes involved in biofilm formation in S. aureus, a model antimicrobial-resistant species. *Journal of Medical Bacteriology*, *7*(3-4), 30–41.

Greco, C., Mastronardi, C., Pagotto, F., Mack, D., & Ramirez-Arcos, S. (2008). Assessment of biofilm-forming ability of coagulase-negative staphylococci isolated from contaminated platelet preparations in Canada. *Transfusion*, *48*(5), 969–977.

Hassan, S., El-Shaer, A., Oraby, A., & Salim, E. (2023). Investigations of charge extraction and trap-assisted recombination in polymer solar cells via hole transport layer doped with NiO nanoparticles. *Optical Materials*, *145*, 114413.

Hindieh, P., Yaghi, J., Assaf, J. C., Chokr, A., Atoui, A., Tzenios, N., Louka, N., & El Khoury, A. (2025). Emerging multimodal strategies for bacterial biofilm eradication: a comprehensive review. *Microorganisms*, *13*(12), 2796.

Jangid, P., Meena, A., Prerna, R., Hashmi, Z. H., Kumar, V., & Bhagtani, H. (2025). The role of artificial intelligence in safeguarding patient privacy in healthcare systems. *Journal of Pharmacy & Bioallied Sciences*, *17*(Suppl 2), S1083.

Kalita, C., Sarkar, R. D., Verma, V., Bharadwaj, S. K., Kalita, M. C., Boruah, P. K., Das, M. R., & Saikia, P. (2021). Bayesian modeling coherenced green synthesis of NiO nanoparticles using camellia sinensis for efficient antimicrobial activity. *BioNanoScience*, *11*(3), 825–837.

Karthik, K., Dhanuskodi, S., Gobinath, C., Prabukumar, S., & Sivaramakrishnan, S. (2018). Multifunctional properties of microwave assisted CdO–NiO–ZnO mixed metal oxide nanocomposite: enhanced photocatalytic and antibacterial activities. *Journal of Materials Science: Materials in Electronics*, *29*(7), 5459–5471.

Kaur, P. (2018). Biosynthesis of nanoparticles using eco-friendly factories and their role in plant pathogenicity: a review. *Biotechnology Research and Innovation*, *2*(1), 63–73.

Khalifa, M. J. (2025). Green Synthesis of Copper Oxide Nanoparticles Using Urtica Dioica Leaf Extract. *Journal of Multidisciplinary*, *5*(01), 1–4.

Khan, N. A., Saeed, K., Khan, I., Gul, T., Sadiq, M., Uddin, A., & Zekker, I. (2022). Efficient photodegradation of orange II dye by nickel oxide nanoparticles and nanoclay supported nickel oxide nanocomposite. *Applied Water Science*, *12*(6), 131.

Kim, J., Kim, M., Kim, S., & Ryu, S. (2017). Sensitive detection of viable Escherichia coli O157: H7 from foods using a luciferase-reporter phage phiV10lux. *International journal of food microbiology*, *254*, 11–17.

Lawal, A., Kabir, L. M., Balarabe, F. T., Abubakar, Y., Usman, M. D., Lawal, F. Y., & Umar, Y. M. (2025). Isolation and characterization of shiga toxin-producing Escherichia coli O157: H7 from cattle feces within

Zaria Metropolis, Nigeria. *Microbes and Infectious Diseases*, *6*(3), 5020–5028.

Livak, K. J., & Schmittgen, T. D. (2001). Analysis of relative gene expression data using real-time quantitative PCR and the 2− ΔΔCT method. *methods*, *25*(4), 402–408.

Lopes, N., Freitas, A. I., Ramos, H., & Vasconcelos, C. (2021). S. epidermidis isolates from a tertiary care Portuguese hospital show very high antibiotic non-susceptible rates and significant ability to form biofilms. *Applied Microbiology*, *1*(1), 150–161.

Magdy, N., Ezzat, D. T., Dawood, M. E., Moustafa, M. M., & Ghany, K. A. E. (2026). Thyme and cinnamon essential oils inhibit multidrug resistant Escherichia coli and Klebsiella pneumoniae and alter virulence transcripts. *Scientific Reports*, *16*(1), 8265.

Mahmud, M., & Rahman, M. S. (2025). A concise review on applications of nickel oxide nanoparticles and their extraction parts. *International Journal of Advanced Biological and Biomedical Research*, *13*(3), 317–340.

Naskar, A., & Kim, K.-s. (2019). Nanomaterials as delivery vehicles and components of new strategies to combat bacterial infections: Advantages and limitations. *Microorganisms*, *7*(9), 356.

Niu, Y., Yu, M., Hartono, S. B., Yang, J., Xu, H., Zhang, H., Zhang, J., Zou, J., Dexter, A., & Gu, W. (2013). Nanoparticles mimicking viral surface topography for enhanced cellular delivery. *Adv. Mater*, *25*(43), 6233–6237.

Nowak, J. A., Cho, E., Davis, M. A., Zheng, S., Bell, L., Sha, F., Magdalenski, J. S., Lui, A., Napoli, M., & Falahat, R. (2026). Strengthening antisense oligonucleotide-mediated anti-tumor immunity via metal–organic framework nanoparticles. *Nano letters*, *26*(8), 2861–2868.

O'Toole, G. A. (2011). Microtiter dish biofilm formation assay. *Journal of Visualized Experiments (JoVE)*(47), e2437.

Organization, W. H. (2022). Optimized broth microdilution plate methodology for drug susceptibility testing of Mycobacterium tuberculosis complex.

Pankey, G. A., & Sabath, L. (2004). Clinical relevance of bacteriostatic versus bactericidal mechanisms of action in the treatment of Gram-positive bacterial infections. *Clinical infectious diseases*, *38*(6), 864–870.

Parvathalu, K., Kumar, D. N., Rajitha, K., Kishan, M. G., Kumar, B. N., Bhemarajam, J., Naidu, S. R., Merlinsheeba, G., Mandal, P., & Banne, S. (2023). Facile synthesis of silver nanoparticles using green tea leaf extract and evolution of antibacterial activity. *Plasmonics*, *18*(5), 1837–1845.

Pérez-Lavalle, L., Valero, A., Cejudo-Gómez, M., & Carrasco, E. (2023). Fate and biofilm formation of Salmonella enterica subsp. enterica serovar Thompson on fresh strawberries stored under refrigeration and room temperatures. *Food Control*, *153*, 109906.

Qais, F. A., Ahmad, I., Altaf, M., Manoharadas, S., Al-Rayes, B. F., Ali Abuhasil, M. S., & Almaroai, Y. A. (2021). Biofabricated silver nanoparticles exhibit broad-spectrum antibiofilm and antiquorum sensing activity against Gram-negative bacteria. *RSC advances*, *11*(23), 13700–13710.

Raghupathi, K. R., Koodali, R. T., & Manna, A. C. (2011). Size-dependent bacterial growth inhibition and mechanism of antibacterial activity of zinc oxide nanoparticles. *Langmuir*, *27*(7), 4020–4028.

Rasheed, A. Y., & F Jum'a, F. (2026). Evaluation of the antioxidant activity of pomegranate peel and green tea tannins loaded with nanoparticles in cryopreserved burgers. *Journal of food science and technology (Iran)*, *23*(174), 175–188.

Ren, G., Hu, D., Cheng, E. W., Vargas-Reus, M. A., Reip, P., & Allaker, R. P. (2009). Characterisation of copper oxide nanoparticles for antimicrobial applications. *International journal of antimicrobial agents*, *33*(6), 587–590.

Rieu, A., Weidmann, S., Garmyn, D., Piveteau, P., & Guzzo, J. (2007). Agr system of Listeria monocytogenes EGD-e: role in adherence and differential expression pattern. *Applied and Environmental Microbiology*, *73*(19), 6125–6133.

Sajid, A., Manzoor, Q., Javed, R., Fatima, A., Shehzada, M. A. A., Sajid, A., Sadiqa, A., Ahmad, A., & Mele, G. (2026). A green synthesis of Sm doped NiO nano catalyst as dual functional material for photocatalytic degradation and electrochemical sensing. *Scientific Reports*.

Sankar, A. U. R., Kiran, Y., Mohan, V. M., Kumar, A. K., & Varalakshmi, M. V. (2023). Green synthesis of cotton flower shaped nickel oxide nanoparticles: Anti-bacterial and tribological studies. *Inorganic Chemistry Communications*, *157*, 111239.

Sati, A., Ranade, T. N., Mali, S. N., Ahmad Yasin, H. K., & Pratap, A. (2025). Silver Nanoparticles (AgNPs): Comprehensive Insights into Bio/Synthesis, Key Influencing Factors, Multifaceted Applications, and Toxicity A 2024 Update. *ACS omega*, *10*(8), 7549–7582.

Şensoy Gün, B., Gurbanov, R., & Tunalı, B. (2025). Biofilm-inhibiting ZnO@ Eggshell nanocomposites: green synthesis, characterization, and biomedical potential. *Biometals*, *38*(5), 1447–1468.

Shao, B., Shang, X., Yang, Q., Li, C., Zhao, F., & Ju, J. (2026). Green nanotechnology: Harnessing metal and its oxide nanoparticles to overcome microbial resistance. *Advanced Composites and Hybrid Materials*, *9*(2), 178.

Sharma, A., Kumar, N., Dhanda, A., Yadav, A., & Aggarwal, N. K. (2024). In vivo assessment of antimicrobial, antioxidant, antigenotoxic and antimutagenic effects of different extracts from Camellia sinensis. *Systems Microbiology and Biomanufacturing*, *4*(1), 282–293.

Singh, J., Dutta, T., Kim, K.-H., Rawat, M., Samddar, P., & Kumar, P. (2018). 'Green'synthesis of metals and their oxide nanoparticles: applications for environmental remediation. *Journal of nanobiotechnology*, *16*(1), 84.

Sirelkhatim, A., Mahmud, S., Seeni, A., Kaus, N. H. M., Ann, L. C., Bakhori, S. K. M., Hasan, H., & Mohamad, D. (2015). Review on zinc oxide nanoparticles: antibacterial activity and toxicity mechanism. *Nano-micro letters*, *7*(3), 219–242.

Slavin, Y. N., Asnis, J., Häfeli, U. O., & Bach, H. (2017). Metal nanoparticles: understanding the mechanisms behind antibacterial activity. *Journal of nanobiotechnology*, *15*(1), 65.

Solati, S. M., Tajbakhsh, E., Khamesipour, F., & Gugnani, H. C. (2015). Prevalence of virulence genes of biofilm producing strains of Staphylococcus epidermidis isolated from clinical samples in Iran. *AMB Express*, *5*(1), 47.

Spaggiari, C. (2025). Innovative techniques for the extraction and characterization of natural products for health applications.

Stepanović, S., Vuković, D., Dakić, I., Savić, B., & Švabić-Vlahović, M. (2000). A modified microtiter-plate test for quantification of staphylococcal biofilm formation. *Journal of microbiological methods*, *40*(2), 175–179.

Tahir, I., Amina, S. J., Ahmad, N. M., & Janjua, H. A. (2024). Antimicrobial coating of biologically synthesized silver nanoparticles on surgical fabric and surgical blade to prevent nosocomial infections. *Heliyon*, *10*(17).

Tanaka, T., Matsuo, Y., & Kouno, I. (2009). Chemistry of secondary polyphenols produced during processing of tea and selected foods. *International journal of molecular sciences*, *11*(1), 14–40.

Tian, X., Chen, H., Ren, D., & Yang, X. (2026). Selenium nanoparticles driving innovations across the food chain: applications in food systems, feed supplementation, and sustainable agriculture. *Journal of Agricultural and Food Chemistry*, *74*(7), 5941–5961.

Uddin, S., Safdar, L. B., Anwar, S., Iqbal, J., Laila, S., Abbasi, B. A., Saif, M. S., Ali, M., Rehman, A., & Basit, A. (2021). Green synthesis of nickel oxide nanoparticles from Berberis balochistanica stem for investigating bioactivities. *Molecules*, *26*(6), 1548.

Wagner, M. R., Busby, P. E., & Balint-Kurti, P. (2020). Analysis of leaf microbiome composition of near-isogenic maize lines differing in broad-spectrum disease resistance. *New Phytologist*, *225*(5), 2152–2165.

Wiegand, I., Hilpert, K., & Hancock, R. E. (2008). Agar and broth dilution methods to determine the minimal inhibitory concentration (MIC) of antimicrobial substances. *Nature protocols*, *3*(2), 163–175.

Yaqoob, S. B., Adnan, R., Rameez Khan, R. M., & Rashid, M. (2020). Gold, silver, and palladium nanoparticles: a chemical tool for biomedical applications. *Frontiers in chemistry*, *8*, 376.

Zhang, S., Lin, L., Huang, X., Lu, Y.-G., Zheng, D.-L., & Feng, Y. (2022). Antimicrobial properties of metal nanoparticles and their oxide materials and their applications in oral biology. *Journal of Nanomaterials*, *2022*(1), 2063265.

Zheng, J., Clogston, J. D., Patri, A. K., Dobrovolskaia, M. A., & McNeil, S. E. (2011). Sterilization of silver nanoparticles using standard gamma irradiation procedure affects particle integrity and biocompatibility. *Journal of nanomedicine & nanotechnology*, *2011*(Suppl 5), 001.

Zhishen, J., Mengcheng, T., & Jianming, W. (1999). The determination of flavonoid contents in mulberry and their scavenging effects on superoxide radicals. *Food chemistry*, *64*(4), 555–559.

How to cite this paper:

Basbus Khanevaneh, M., Mirpour, M., Faezi Ghasemi, M., & Rasti, B. (n.d.). Green-synthesized nickel oxide nanoparticles from tea: A dual-action antibiofilm and anti-quorum-sensing activity against selected foodborne pathogens. *Microbiology, Metabolites and Biotechnology, 9*(2), 2026-1-21.
DOI: 10.22104/mmb.2026.8491.1212